JOURNAL OF NEUROPHYSIOLOGY
Vol. 76, No. 3, September 1996. *Printed in U.S.A.*

# Ionic Mechanisms Underlying Synchronized Oscillations and Propagating Waves in a Model of Ferret Thalamic Slices

ALAIN DESTEXHE, THIERRY BAL, DAVID A. McCORMICK, AND TERRENCE J. SEJNOWSKI
*Department of Physiology, Laval University School of Medicine, Quebec G1K 7P4, Canada; Institut Alfred Fessard, Centre National de la Recherche Scientifique, Gif-sur-Yvette Cedex 91198, France; Section of Neurobiology, Yale University School of Medicine, New Haven, Connecticut 06510; The Howard Hughes Medical Institute and The Salk Institute, Computational Neurobiology Laboratory, La Jolla, California 92037; and Department of Biology, University of California San Diego, La Jolla, California 92037*

## SUMMARY AND CONCLUSIONS

*1*. A network model of thalamocortical (TC) and thalamic reticular (RE) neurons was developed based on electrophysiological measurements in ferret thalamic slices. Single-compartment TC and RE cells included voltage- and calcium-sensitive currents described by Hodgkin-Huxley type of kinetics. Synaptic currents were modeled by kinetic models of $\alpha$-amino-3-hydroxy-5-methyl-4-isoxazolepropionic acid (AMPA), $\gamma$-aminobutyric acid-A ($GABA_A$) and $GABA_B$ receptors.

*2*. The model reproduced successfully the characteristics of spindle and slow bicuculline-induced oscillations observed in vitro. The characteristics of these two types of oscillations depended on both the intrinsic properties of TC and RE cells and their pattern of interconnectivity.

*3*. The oscillations were organized by the reciprocal recruitment between TC and RE cells, due to their mutual connectivity and bursting properties. TC cells elicited AMPA-mediated excitatory postsynaptic potentials (EPSPs) in RE cells, whereas RE cells elicited a mixture of $GABA_A$ and $GABA_B$ inhibitory postsynaptic potentials (IPSPs) in TC cells. Because of the presence of a T current, sufficiently strong EPSPs could elicit a burst in RE cells, and TC cells could generate a rebound burst following GABAergic IPSPs. Under these conditions, interaction between the TC and RE cells produced sustained oscillations.

*4*. In the absence of spontaneous oscillation in any cell, the TC-RE network remained quiescent. Spindle oscillations with a frequency of 9–11 Hz could be initiated by stimulation of either TC or RE neurons. A few spontaneously oscillating TC neurons recruited the entire network model into a "waxing-and-waning" oscillation. These "initiator" cells could be an extremely small proportion of TC cells.

*5*. In intracellular recordings, TC cells display a reduced ability for burst firing after a sequence of bursts. The "waning" phase of spindles was reproduced in the network model by assuming an activity-dependent upregulation of $I_h$ operating via a calcium-binding protein in TC cells, as shown previously in a two-cell model.

*6*. Following the global suppression of $GABA_A$ inhibition, the disinhibited RE cells produced prolonged burst discharges that elicited strong $GABA_B$-mediated currents in TC cells. The enhancement of slow IPSPs in TC cells was also due to cooperativity in the activation of $GABA_B$-mediated current. These slow IPSPs recruited TC and RE cells into slower waxing-and-waning oscillations (3–4 Hz) that were even more highly synchronized.

*7*. Local axonal arborization of the TC to RE and RE to TC projections allowed oscillations to propagate through the network. An oscillation starting at a single focus induced a propagating wavefront as more cells were recruited progressively. The waning of the oscillation also propagated due to upregulation of $I_h$ in TC cells, leading to waves of spindle activity as observed in experiments.

*8*. The spatiotemporal properties of propagating waves in the model were highly dependent on the intrinsic properties of TC cells. The spatial pattern of spiking activity was markedly different for spindles compared with bicuculline-induced oscillations and depended on the rebound burst behavior of TC cells. The upregulation of $I_h$ produced a refractory period so that colliding spindle waves merged into a single oscillation and extinguished. Finally, reducing the $I_h$ conductance led to sustained oscillations.

*9*. Two key properties of cells in the thalamic network may account for the initiation, propagation, and termination of spindle oscillations, the activity-dependent upregulation of $I_h$ in TC cells, and the localized axonal projections between TC and RE cells. In addition, the model predicts that a nonlinear stimulus dependency of $GABA_B$ responses accounts for the genesis of prolonged synchronized discharges following block of $GABA_A$ receptors.

## INTRODUCTION

Synchronous oscillations are commonly observed in the thalamus during sleep or deep anesthesia. Sleep spindles in particular have been investigated thoroughly using extracellular and intracellular recordings in thalamic cells (Andersen and Andersson 1968; Bal et al. 1995a,b; Steriade and Deschênes 1984). The anatomic and morphological features of thalamic nuclei have been also very well documented (for a review, see Jones 1985). More recent studies (reviewed in McCormick 1992) have revealed a variety of receptor types and intrinsic currents in thalamic cells, whose activation characteristics are now beginning to be understood in detail. Taken together, these data make the thalamus a structure for which computational models can be extremely useful in testing the range of possible interactions (reviewed in Destexhe and Sejnowski 1997).

Spindle oscillations depend on the integrity of intrathalamic connectivity as they do not appear in thalamic nuclei deprived (naturally or artificially) from afferents from the thalamic reticular (RE) nucleus (Steriade et al. 1985). Investigations of an in vitro model of spindling activity have clarified the cellular mechanisms underlying spindle rhythmicity in slices (Bal et al. 1995a,b; von Krosigk et al. 1993). It currently is believed that spindle oscillations result from a reciprocal interaction between thalamocortical (TC) relay cells and RE cells. In this interaction, both intrinsic and

synaptic properties play critical roles. The bursting properties of thalamic cells, mainly due to the low-threshold current $I_T$, their level of membrane potential, and the types of receptor mediating their synaptic interactions, are all essential components of the genesis of rhythmicity (Steriade et al. 1993b).

Several fundamental properties of spindles remain poorly understood. One of these is how spindles are initiated and propagated through the network, as well as how they terminate, leading to the so-called "waxing-and-waning" pattern so typical of spindle waves. Recent in vivo and in vitro studies have explored how these oscillations are distributed in different brain structures (Steriade et al. 1996). In particular, a recent investigation of propagating properties of spindles in ferret thalamic slices (Kim et al. 1995) showed that spindle oscillations consistently propagate in the dorsal-ventral axis.

These experiments suggest the following scenario for how spindles are organized. Burst discharges in TC cells evoke barrages of $\alpha$-amino-3-hydroxy-5-methyl-4-isoxazolepropionic acid (AMPA)-receptor-mediated excitatory postsynaptic potentials (EPSPs) in RE cells. These EPSPs activate $I_T$ and elicit burst discharges in RE cells, which in turn evoke GABAergic inhibitory postsynaptic potentials (IPSPs) in TC cells. These IPSPs deinactivate $I_T$ and elicit burst discharges, and the same cycle starts again. A spindle could be started by the spontaneous discharge of either TC or RE cells and propagate through the recruitment of adjacent cells through localized axonal projections. The mechanisms of termination of spindle waves still remains to be determined.

In this paper, we investigated model networks of TC and RE cells, endowed with intrinsic properties and topographic connectivity specific to the thalamus. The model reproduced the propagating properties of spindle waves, in agreement with another modeling study (Golomb et al. 1996) that used simpler models of thalamic neurons (no action potentials and graded synaptic transmission). The focus of the Golomb et al. model was the parameters that influence propagation of activity, but mechanisms for the initiation and termination of spindle oscillations were not included.

We investigated the hypothesis that the termination, or waning, of spindles depends on an activity-dependent process in TC cells. Based on recent experiments by Bal and McCormick (1996), we assume that the calcium-dependent upregulation of a hyperpolarization-activated current, $I_h$, is the biophysical basis of the waning. We show that this mechanism, together with other known intrinsic and synaptic properties of the thalamic circuitry, accounts for the initiation, propagation, and termination of spindle waves.

We also show that the same model exhibits the patterns of oscillation observed after application of bicuculline, a $\gamma$-aminobutyric acid-A ($GABA_A$)-receptor antagonist. This convulsant transforms spindles into slower and more synchronized oscillations (Bal et al. 1995a,b; Kim et al. 1995; von Krosigk et al. 1993), similar to the pattern seen in thalamic neurons during some types of epileptic discharges. In agreement with previous models (Destexhe and Sejnowski 1995; Golomb et al. 1996), lateral inhibition in the RE nucleus was essential in developing such patterns of discharges.

Some of the results presented here were reported previously in an abstract (Destexhe et al. 1995).

## METHODS

The network model studied here was based on kinetic models of TC and RE neurons that were modified from previous models (Destexhe and Sejnowski 1995; Destexhe et al. 1993a,b, 1994a, 1996; Huguenard and McCormick 1992; McCormick and Huguenard 1992). Only those currents that were needed to account for the genesis of spindle and bicuculline-induced synchronized oscillations were included.

### *Cable geometry and intrinsic currents*

Each cell had a single compartment, with the membrane potential governed by the following cable equation

$$C_m\dot{V}_T = -g_L(V_T - E_L) - I_T - I_h - I_{KL} - I_{Na} - I_K - I_{GABA_AT} - I_{GABA_B} \quad (1)$$

$$C_m\dot{V}_R = -g_L(V_R - E_L) - I_{Ts} - I_{Na} - I_K - I_{AMPA} - I_{GABA_AR} \quad (2)$$

where $V_T$ and $V_R$ are the membrane potentials of TC and RE cells, respectively, and $C_m = 1\ \mu F/cm^2$ is the specific capacity of the membrane, $g_L$ is the leakage conductance, $E_L$ is the leakage reversal potential, $I_T$ and $I_{Ts}$ are the low-threshold calcium currents, $I_h$ is the hyperpolarization-activated cation current, $I_{KL}$ is a leak potassium current, $I_{Na}$ and $I_K$ are the sodium and potassium currents responsible for action potentials, and the synaptic currents are $I_{GABA_AT}$ and $I_{GABA_B}$ associated, respectively, with $GABA_A$ and $GABA_B$ receptors in the synapses from RE to TC, $I_{AMPA}$ for the AMPA/kainate receptors from TC to RE cells, and $I_{GABA_AR}$ for $GABA_A$ receptors between RE cells. All intrinsic currents in this model are variants from the same generic equation

$$I_j = \bar{g}_j m^M h^N (V - E_j) \quad (3)$$

where the current $I_j$ is expressed as the product of respectively the maximal conductance, $\bar{g}_j$, activation ($m$) and inactivation variables ($h$), and the difference between the membrane potential $V$ and the reversal potential $E_j$. The gating of the channel is derived from the following first order kinetic scheme

$$C \underset{\beta(V)}{\overset{\alpha(V)}{\rightleftharpoons}} O \quad (4)$$

where $O$ and $C$ are the open and closed states of the gate. The variables $m$ and $h$ represent the fraction of independent gates in the open state, following the convention introduced by Hodgkin and Huxley (1952). The steady state activation and the time constant, respectively, are given by $m_\infty = \alpha/(\alpha + \beta)$ and $\tau_m = 1/(\alpha + \beta)$, and similarly for $h$.

The model of the RE cell was a single compartment reduction obtained from a detailed compartmental model of RE neurons (Destexhe et al. 1996). The length and diameter of the single compartment were of 70 and 65 $\mu$m, respectively (area of $\sim$14,300 $\mu m^2$). The passive properties were obtained from directly fitting the model to capacitive transients recorded in a RE cell to give correct input resistance and time constant (Destexhe et al. 1996). Passive parameters were $g_L = 0.05\ mS/cm^2$ and $E_L = -90\ mV$.

For active currents, only the low-threshold $Ca^{2+}$ current of RE cells, $I_{Ts}$, was considered; other currents, such as $I_{K[Ca]}$ and $I_{CAN}$ were not included for simplicity. Although these currents have important consequences in shaping the firing patterns of single RE cells (Bal and McCormick 1993), we found that they had very little influence on network behavior (see also Destexhe et al. 1994a). The kinetics of $I_{Ts}$ were derived from voltage-clamp data on rat RE cells using a $m^2h$ formalism (Huguenard and Prince

1992) and were given in detail in a previous paper (Destexhe et al. 1996). The amplitude of the current was obtained by fitting the model to current-clamp and voltage-clamp recordings of $I_{Ts}$ in RE cells (Destexhe et al. 1996) and the maximal conductance of the current was of $\bar{g}_{Ts} = 3$ mS/cm$^2$.

Intracellular $Ca^{2+}$ dynamics was modeled by a simple first-order decay with a time constant of 5 ms (as in McCormick and Huguenard 1992); the equilibrium $Ca^{2+}$ concentrations were 2 mM extracellularly and 240 nM intracellularly, which corresponds to a reversal potential of ~120 mV. $I_{Na}$ and $I_K$ were described by kinetic equations identical to hippocampal pyramidal cells from Traub and Miles (1991).

The model of the TC cell was based on previous models (Destexhe et al. 1993a; Huguenard and McCormick 1992; McCormick and Huguenard 1992) with some important differences. The geometry and passive properties were taken from McCormick and Huguenard (1992): the length and diameter of the single compartment were of 96 $\mu$m each (surface of ~29,000 $\mu$m$^2$), and the passive currents were of $g_L = 0.01$ mS/cm$^2$, $E_L = -70$ mV and $I_{KL}$ had a maximal conductance between 2 and 8 nS. These values give a correct input resistance and time constant of the cell (see McCormick and Huguenard 1992).

Active currents in TC cells were the low-threshold $Ca^{2+}$ current, $I_T$, and the hyperpolarization-activated current, $I_h$. $I_T$ was modeled by kinetics similar to the model introduced by Huguenard and McCormick (1992), using a $m^2h$ formalism, with activation ($m$) considered at steady state and inactivation ($h$) described by a first-order equation. The time constant of inactivation ($\tau_h$) was fit by a double exponential expression to the voltage-clamp data of Huguenard and Prince (1992), so that

$$\tau_h(V) = 30.8 + \{211.4 + \exp[(V + 113.2)/5]\}/\{1 + \exp[(V + 84)/3.2]\} \quad (5)$$

at a temperature of 24°C. The temperature was adjusted to 36°C using a $Q_{10}$ factor of 3 (Coulter et al. 1989). The maximal conductance of $I_T$ was of $g_T = 2$ mS/cm$^2$ and $Ca^{2+}$ dynamics was identical to those in RE cells.

A potassium A current ($I_A$) is present in TC cells (Huguenard et al. 1991) and delays spike generation (McCormick and Huguenard 1992) by increasing the threshold for action potentials (Rush and Rinzel 1994). This current was not incorporated here, but a positive shift of 20 mV in action potential threshold was included in TC cells to mimic the effect of the A current during bursting activity. In a model of single spike mode in TC cells, an explicit representation of this current would be needed (McCormick and Huguenard 1992). The inclusion of a higher threshold for action potentials had very little effect on network behavior but gave more realistic simulated bursts.

$I_h$ was modeled with a single-variable kinetic scheme ($m$ formalism) based on previous models for the dependence of its activation on voltage and intracellular $Ca^{2+}$. The voltage dependence of $I_h$ was based on voltage-clamp data of this current in TC cells (McCormick and Pape 1990a), and the rate constants used were identical to those in the model introduced by Huguenard and McCormick (1992). The regulation of $I_h$ by intracellular $Ca^{2+}$ was based on voltage-clamp data from the hyperpolarization-activated current in sino-atrial cells. This current, which is similar to $I_h$ in thalamic neurons, has a strong $Ca^{2+}$ dependence (Hagiwara and Irisawa 1989) but calcium may not bind directly to the channel (Zaza et al. 1991). The model used here was a modified version of a kinetic model introduced previously (Destexhe et al. 1993a). The previous model considered the direct binding of $Ca^{2+}$ ions to the open form of the channel. In the present model, we assume that the voltage dependence and conductance is influenced by $Ca^{2+}$ indirectly through the binding of $Ca^{2+}$ to a regulating factor (P), which itself binds to the open form of the channel and blocks its

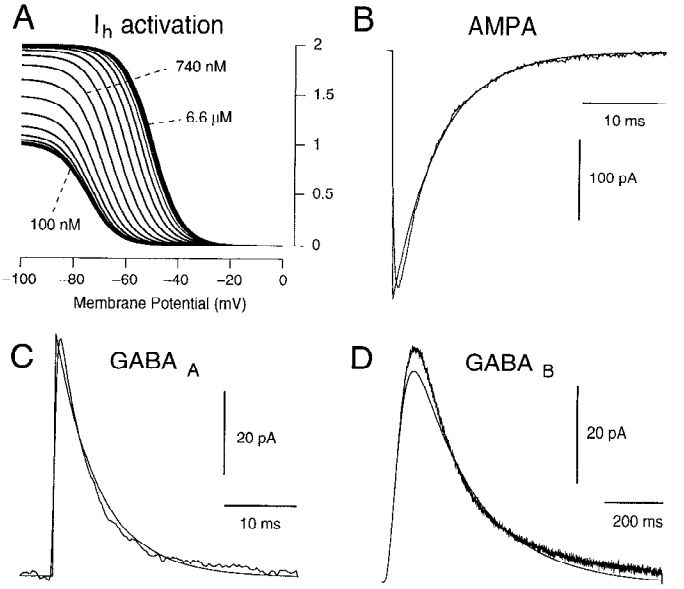


FIG. 1. Kinetic models for $I_h$ and synaptic currents. *A*: voltage-dependent activation of $I_h$ for different intracellular calcium concentrations. Successive traces from *bottom to top* indicate activation curve ($[O] + g_{inc}[O_L]$) for different intracellular $Ca^{2+}$ increasing from 100 nM to 6.6 M by a factor of 1.2 (multiplicative). Regulation of $I_h$ by $Ca^{2+}$ operated through a regulatory protein that had 4 binding sites for $Ca^{2+}$ and regulated the channel by binding to its open form, resulting in a shift of voltage dependence of $I_h$ as well as an increase of total conductance. *B*: kinetic model for glutamatergic synaptic currents on $\alpha$-amino-3-hydroxy-5-methyl-4-isoxazolepropionic acid (AMPA) receptors compared with whole cell recordings of AMPA-receptor-mediated currents obtained in mossy fiber synapses in CA3 pyramidal cells (Xiang et al. 1992) (recorded at 31°C). *C*: kinetic model for $\gamma$-aminobutyric acid-A ($GABA_A$)-receptor-mediated currents compared with whole cell recordings of $GABA_A$ currents obtained in dentate granule cells (from Otis and Mody 1992). *D*: kinetic model for $GABA_B$-mediated currents compared with whole cell recordings of $GABA_B$ currents obtained in dentate granule cells (from Otis et al. 1993) (*C* and *D* recorded at 33–35°C). In *B–D*, continuous traces show the best fit obtained after running a simplex procedure to optimize the parameters of the kinetic model; noisy traces are averages of whole cell recordings of postsynaptic currents obtained by extracellular stimulation in vitro. Models in *B* and *C* used 0.3-ms pulses of transmitter at a concentration of 0.5 mM. Because of cooperative properties of $GABA_B$ responses, a single short pulse was insufficient to evoke detectable currents (Destexhe and Sejnowski 1995), and a longer pulse of 5 ms was used to fit the data in *D*.

transition to the closed form. This leads to an effective shift of the voltage dependence to more depolarized values (Fig. 1*A*), as observed experimentally (Hagiwara and Irisawa 1989).

The full kinetic scheme was

$$C \underset{\beta(V)}{\overset{\alpha(V)}{\rightleftarrows}} O \quad (6)$$

$$P_0 + 2Ca^{2+} \underset{k_2}{\overset{k_1}{\rightleftarrows}} P_1 \quad (7)$$

$$O + P_1 \underset{k_4}{\overset{k_3}{\rightleftarrows}} O_L \quad (8)$$

where the first reaction represents the voltage-dependent transitions of $I_h$ channels between closed ($C$) and open ($O$) forms, with $\alpha$ and $\beta$ as transition rates. The second reaction represents the binding of intracellular $Ca^{2+}$ ions to a regulating factor ($P_0$ for unbound and $P_1$ for bound) with four binding sites for calcium and rates of $k_1 = 2.5 \times 10^7$ mM$^{-4}$ ms$^{-1}$ and $k_2 = 4 \times 10^{-4}$ ms$^{-1}$ (half-activation of 0.002 mM $Ca^{2+}$). The calcium-bound form $P_1$ associates with the open form of the channel, leading to a "locked"

open form $O_L$, with rates of $k_3 = 0.1$ ms$^{-1}$ and $k_4 = 0.001$ ms$^{-1}$. The current is then proportional to the relative concentration of open channels

$$I_h = \bar{g}_h([O] + g_{inc}[O_L])(V - E_h) \quad (9)$$

with a maximal conductance of $\bar{g}_h = 0.02$ mS/cm$^2$ and a reversal potential of $E_h = -40$ mV. Because of the factor $g_{inc} = 2$, the conductance of the calcium-bound open state of $I_h$ channels is twice that of the unbound open state. This produces an augmentation of conductance after the binding of $Ca^{2+}$, as observed in sino-atrial cells (Hagiwara and Irisawa 1989).

### *Synaptic currents*

Kinetic models of synaptic currents were directly fit to experimental data (Destexhe and Sejnowski 1995; Destexhe et al. 1994c,d) based on whole cell recorded synaptic currents obtained in hippocampal neurons (Otis and Mody 1992; Otis et al. 1993; Xiang et al. 1992). In particular, AMPA and $GABA_A$ receptor-mediated currents were both represented by a simple first-order activation scheme

$$C + T \underset{\beta}{\overset{\alpha}{\rightleftarrows}} O \quad (10)$$

where the transition between the closed ($C$) and open ($O$) states depends on the binding of transmitter ($T$). We assumed that the concentration of $T$ is a pulse that is 0.3 ms in duration and 0.5 mM in amplitude following an action potential in the presynaptic neuron. This brief pulse is consistent with estimates of the time course of transmitter in the synaptic cleft (Clements et al. 1992; Destexhe and Sejnowski 1995). Corroboration also is found in experimentally applied pulses of agonist to membrane patches that mimic the time course of synaptic currents (Colquhoun et al. 1992). The rate constants were estimated from fitting the model to experimentally recorded AMPA and $GABA_A$ currents: $\alpha = 0.94$ ms$^{-1}$mM$^{-1}$, $\beta = 0.18$ ms$^{-1}$ for AMPA (Fig. 1*B*) and $\alpha = 20$ ms$^{-1}$mM$^{-1}$, $\beta = 0.16$ ms$^{-1}$ for $GABA_A$-mediated currents (Fig. 1*C*).

The current then was given by

$$I_{syn} = \bar{g}_{syn}[O](V - E_{syn}) \quad (11)$$

where $I_{syn}$ represents either $I_{AMPA}$, $I_{GABA_AT}$, or $I_{GABA_AR}$; $g_{syn}$ represents, respectively, $g_{AMPA}$, $g_{GABA_AT}$, or $g_{GABA_AR}$; $[O]$ is the fraction of open channels, and the reversal potential $E_{syn}$ was 0 mV for $I_{AMPA}$ and $-85$ mV for $I_{GABA_AT}$ and $I_{GABA_AR}$.

$GABA_B$ receptors have a more complex scheme of activation that involves the activation of $K^+$ channels by G proteins (Dutar and Nicoll 1988). Our model was based on cooperativity in the activation of $K^+$ channels, which need several G-protein binding to be activated. We used a modified version of a kinetic model of the $GABA_B$ current introduced previously (Destexhe and Sejnowski 1995; Destexhe et al. 1994d)

$$R_0 + T \rightleftharpoons R \rightleftharpoons D \quad (12)$$

$$R + G_0 \rightleftharpoons RG \rightarrow R + G \quad (13)$$

$$G \rightarrow G_0 \quad (14)$$

$$C_1 + 4G \rightleftharpoons O \quad (15)$$

where the transmitter, $T$, binds to the receptor, $R_0$, leading to its activated form, $R$, and desensitized form, $D$. The G protein is transformed from an inactive (GDP-bound) form, $G_0$, to an activated form, $G$, catalyzed by $R$. Finally, G binds to open the $K^+$ channel, with four independent binding sites. If we assume quasi-stationarity in *Eqs. 13* and *15*, neglect desensitization, and consider $G_0$ in excess, then the kinetic model for this system reduces to

$$\frac{d[R]}{dt} = K_1[T](1 - [R]) - K_2[R]$$

$$\frac{d[G]}{dt} = K_3[R] - K_4[G]$$

$$I_{GABA_B} = \bar{g}_{GABA_B}\frac{[G]^4}{[G]^4 + K_d}(V - E_K)$$

where $[R]$ is the fraction of activated receptor, $[G]$ (in micromolar) is the concentration of activated G protein, $\bar{g}_{GABA_B}$ is the maximal conductance of $K^+$ channels, $E_K = -95$ mV is the potassium reversal potential, and $K_d$ is the dissociation constant of the binding of $G$ on the $K^+$ channels. Direct fitting of the model to whole cell recorded $GABA_B$ currents (Fig. 1*D*) gave the following values: $K_d = 100$ $\mu$M$^4$, $K_1 = 0.5$ mM$^{-1}$ms$^{-1}$, $K_2 = 0.0012$ ms$^{-1}$, $K_3 = 0.18$ ms$^{-1}$, and $K_4 = 0.034$ ms$^{-1}$.

The main difference between this model and that proposed previously (Destexhe and Sejnowski 1995) is the absence of desensitized state for the receptor and the use of short pulses of transmitter of 0.3 ms. We found that the desensitized state was necessary to account accurately for the time course of $GABA_B$ currents, but had little influence on network behavior (not shown). The resulting model involves only two independent variables and is computationally much faster.

### *Estimation of parameters*

All simulations were run using NEURON (Hines 1993) using a temperature of 36°C. The values of parameters for synaptic currents were obtained by fitting the kinetic model directly to experimental recordings using a simplex algorithm (Press et al. 1986), from different initial conditions, until the model converged to the data with stable values for the parameters (Fig. 1, *B–D*).

The passive properties of the RE cell were obtained from directly fitting the model to capacitive transients recorded in an RE cell (see Destexhe et al. 1996). Passive properties of the TC cell were similar to a previous model (McCormick and Huguenard 1992). These values gave correct input resistance and time constants for both types of cells.

Conductance values were consistent with previous models and were varied to test the sensitivity of the results at the network level. The results reported here were robust to changes in parameters within a reasonable range. The parameters that were found to be critically important are discussed explicitly.

### *In vitro recordings*

Intracellular recordings were obtained in ferret thalamic slices, which contained the lateral geniculate laminae, the perigeniculate sector of the reticular nucleus, and the interconnectivity between them. Slice preparation and recording methods were identical to those previously described in detail (Bal et al. 1995a,b; Kim et al. 1995; von Krosigk et al. 1993). All recordings were done at a temperature of 34–35°C.

## RESULTS

We present first the properties of single cells and small circuits and then focus on network properties and spatiotemporal patterns of activity.

### *Small circuits of thalamic reticular neurons*

The burst discharges of RE cells are dominated by the T current, and the shape of the burst depends critically on the lateral $GABA_A$-mediated inhibition between these cells. As shown in Fig. 2*A*, in the presence of lateral inhibition, model

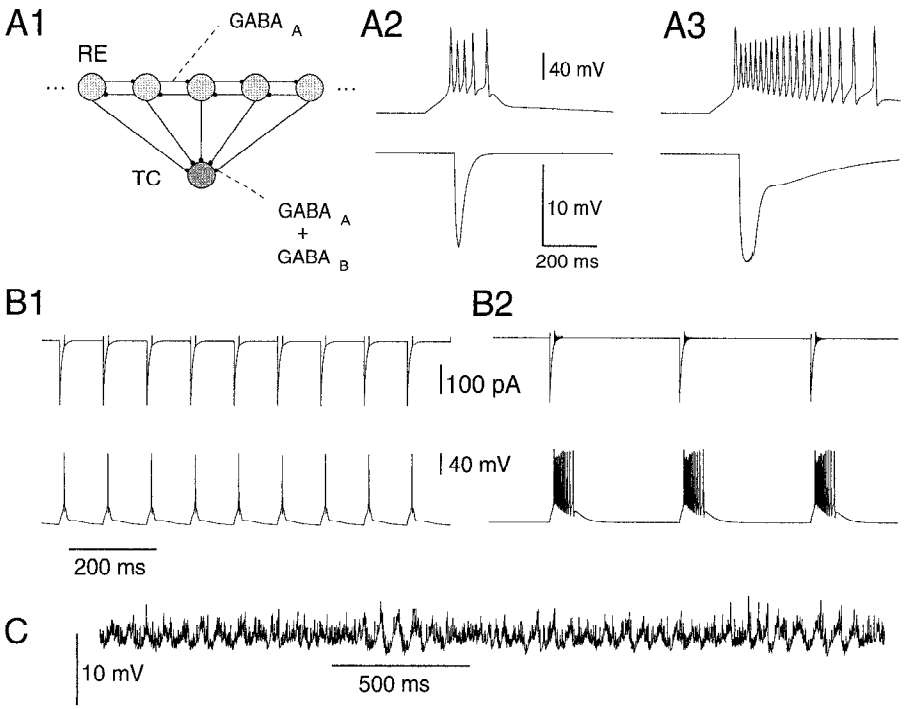


FIG. 2. Oscillatory behavior of reticular thalamic neurons. *A1*: scheme of a 1-dimensional network of thalamic reticular (RE) cells interconnected through $GABA_A$-mediated inhibitory synapses. Each RE cell contacts a thalamocortical (TC) cell through a mixture of $GABA_A$ and $GABA_B$ receptors. *A2*: stimulation of each RE cell by a depolarizing current pulse under normal conditions produced a burst with only a few spikes, which evoked strong $GABA_A$ inhibitory postsynaptic potentials (IPSPs) in TC cells but only a weak $GABA_B$ component. *Top*: burst in a RE cell indicated, and IPSP evoked in target TC cell is shown at *bottom* (*top* has 10 times higher time resolution). *A3*: same simulation without intra-RE inhibition. Stimulation evoked prolonged burst discharges in RE cells, which in turn evoked IPSPs in TC cells that contained a strong $GABA_B$ component (see Destexhe and Sejnowski 1995). *B1*: stimulation of a network of GABAergically connected RE cells at 10 Hz through AMPA receptors can recruit RE cells to burst at same frequency. *B2*: same simulation in absence of intra-RE inhibition. In this case, 3.3 Hz stimulation recruited RE cells in repetitive prolonged burst discharges. *C*: if the membrane potential of RE cells is more depolarized. The average network can show synchronized oscillations at 12–16 Hz. Membrane potential in a 1-dimensional network of 100 RE neurons is shown; 100 RE neurons were depolarized by partial block of leak $K^+$ currents, mimicking the effect of noradrenaline (see also Destexhe et al. 1994b). Total conductances were of 0.2 S for $GABA_A$ in RE cells and 0.02 and 0.04 S for $GABA_A$ and $GABA_B$ in TC cells, respectively.

RE cells produce burst discharges that gave rise to three to seven spikes (Fig. 2*A2, top*), in contrast to the prolonged bursts (15–25 spikes) seen after suppression of $GABA_A$ receptors between RE cells (Fig. 2*A3, top*). These properties are consistent with slice recordings showing that disinhibition in the RE nucleus increases the intensity and duration of burst discharges (Bal et al. 1995b; Huguenard and Prince 1994b; Sánchez-Vives et al. 1995). This observation is also consistent with previous models (Destexhe and Sejnowski 1995; Destexhe et al. 1994a; Golomb et al. 1996).

In thalamic slices, the ratio between $GABA_A$ and $GABA_B$ components in RE-induced IPSPs on target TC cells was shown to depend strongly on the integrity of $GABA_A$-mediated inhibition in the RE nucleus (Huguenard and Prince 1994a; Sánchez-Vives et al. 1995). On the other hand, this ratio was not sensitive to the intensity of stimulation in the RE nucleus (Huguenard and Prince 1994b). These properties are found in the present model because of the kinetic properties of GABAergic receptors (see Destexhe and Sejnowski 1995). Under normal conditions, stimulation in the RE nucleus evoked $GABA_A$-dominated IPSPs in TC cells (Fig. 2*A2*). Blocking $GABA_A$ receptors locally in the RE nucleus enhanced the burst discharges of these cells and evoked a more prominent $GABA_B$ component in TC cells (Fig. 2*A3*).

This enhancement was due to the strong cooperativity in the activation of $GABA_B$ responses (Destexhe and Sejnowski 1995), provided by four independent binding sites of G proteins on the $GABA_B$-associated $K^+$ channels, and is consistent with kinetic studies on G-protein-mediated responses in other systems (Boland and Bean 1993; Golard and Siegelbaum 1993; Yamada et al. 1993). Because of cooperativity, G proteins must be produced at sufficient intracellular concentration to activate the $K^+$ channels. Consequently, a single presynaptic spike is insufficient to evoke a detectable $GABA_B$ current, and prolonged stimulation of $GABA_B$ receptors by GABA must occur to provide a detectable response. The same conclusions hold in simplified models of GABAergic IPSPs based on pulses of transmitter (Fig. 2*A*).

The responses of RE cells to repetitive synaptic stimulation also depended strongly on lateral inhibition between RE cells. Figure 2*B1* shows a 10-Hz stimulation of RE cells through AMPA receptors in the presence of lateral inhibition. The cell shown in the figure responded by producing bursts discharges at 10 Hz with few spikes per burst (1–6

spikes). In the absence of lateral $GABA_A$-mediated inhibition, stimulation at 3.3 Hz recruited RE cells in prolonged bursting discharges (13–25 spikes; Fig. 2*B2*). These two patterns of activity also occurred spontaneously, as described in later sections.

In the absence of external stimulation, or connections with TC cells, an isolated network of RE cells would stay quiescent, consistent with recordings of the isolated RE nucleus in vitro (Bal and McCormick 1993; Bal et al. 1995a,b; Huguenard and Prince 1994b; von Krosigk et al. 1993; Warren et al. 1994). However, in vivo recordings of the deafferented RE nucleus showed spontaneous oscillations (Steriade et al. 1987), which could be reproduced by the model assuming more depolarized RE cells (Destexhe et al. 1994a,b). The present model also produced sustained oscillations if the RE cells were more depolarized (Fig. 2*C*).

*Single thalamocortical cells*

The electrophysiological properties of TC cells are dominated by two voltage-dependent currents, $I_T$ and $I_h$, which allow the cell to produce rebound bursts or spontaneous oscillations (McCormick and Pape 1990a; Soltesz et al. 1991). Neuromodulation can induce the transition between oscillations and a "relay" state in TC cells, through decrease of leak $K^+$ conductances and regulation of the voltage-dependence of $I_h$ (see McCormick 1992). We assume here that, in addition to its voltage dependence and regulation by neuromodulators, $I_h$ also is upregulated by intracellular calcium, which increases transiently as $I_T$ activates during a burst, as described in detail in METHODS.

The model introduced here for upregulation of $I_h$ is similar in spirit to a previous model (Destexhe et al. 1993a), but has important differences. First, $Ca^{2+}$ ions do not bind directly on the channel but through a calcium-binding protein P, which produces a bounded shift of the activation curve (Fig. 1*A*) because P has a maximum concentration inside the cell. Second, the maximal conductance of the channel is now allowed to increase after the binding of P (for $g_{inc} > 1$). These two properties were observed in sino-atrial cells (Hagiwara and Irisawa 1989). On the other hand, the kinetic scheme for voltage dependence here is simpler than in the previous model, which contained a combination of fast and slow activation gates (Destexhe and Babloyantz 1992; Destexhe et al. 1993a). These improvements give a very robust waxing-and-waning behavior to the TC cell.

The single-cell behavior was similar to the previous model (Destexhe et al. 1993a): when the TC cell repetitively bursts, the enhancement of the h current depolarizes the cell, which eventually stops further rebound bursts in the cell. As a consequence, model TC cells show waxing-and-waning slow oscillations, as observed in vitro (Leresche et al. 1991). The dynamics of the TC cell also showed different regimes depending on the balance between $I_T$ and $I_h$ conductances (Fig. 3*A*). For fixed $g_T$, increasing $g_h$ led successively to slow oscillations in the delta range (1–4 Hz), then to waxing-and-waning slow oscillations, and finally, to the relay resting state, consistent with in vitro studies (Soltesz et al. 1991).

During waxing-and-waning, calcium entered through $I_T$ channels at each burst, resulting in an increase of calcium-bound protein ($P_1$) and a gradual increase of $I_h$ channels

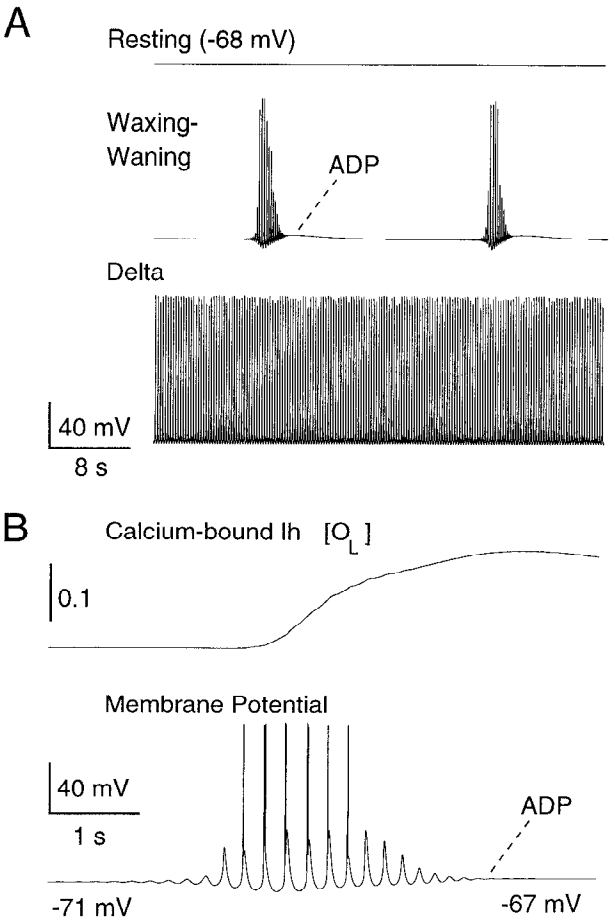


FIG. 3. Intrinsic oscillatory properties of thalamocortical cells. *A*: 3 different modes of TC cells with different conductance values of $I_h$. *Top to bottom*: relay state ($\bar{g}_h$ = 0.025 mS/cm$^2$), slow waxing-and-waning oscillations ($\bar{g}_h$ = 0.02 mS/cm$^2$) and delta oscillations ($\bar{g}_h$ = 0.005 mS/cm$^2$). *B*: intrinsic waxing-and-waning oscillation at higher time resolution. *Top*: fraction of channels in calcium-bound open state ($O_L$) and membrane potential are shown at *bottom*. Leak potassium conductance was of $g_{KL}$ = 5 nS for all simulations.

locked in the open state ($O_L$). This resulted in a progressive afterdepolarization (ADP) at each burst until the cell ceased to oscillate (Fig. 3*B*). This ADP was observed during waxing-and-waning oscillations in TC cells maintained in low magnesium in vitro (Leresche et al. 1991).

In thalamic slices containing both TC and RE cells, intracellularly recorded TC cells exhibit a small (2–5 mV) ADP after repetitive burst discharges (Fig. 4) (Bal and McCormick 1996). This ADP occurred either after spindle oscillations (Bal and McCormick 1996), after bicuculline-induced oscillations (Fig. 4*A*), or after a sequence of hyperpolarizing current pulses (Fig. 4*B*). In the latter case, there was a marked diminution of input resistance in successive responses (Fig. 4, *E* and *F*). This corroborates intracellular recordings of TC cells in vivo showing a diminution of input resistance at the end of spindle sequences (Nunez et al. 1992).

These two properties occurred in the model due to upregulation of $I_h$. In Fig. 5 a current-induced oscillation is compared in a model TC cell with upregulated $I_h$ and in control conditions with nonregulated $I_h$. Successive hyperpolarizing pulses at 4 Hz evoked rebound bursts with a progressive

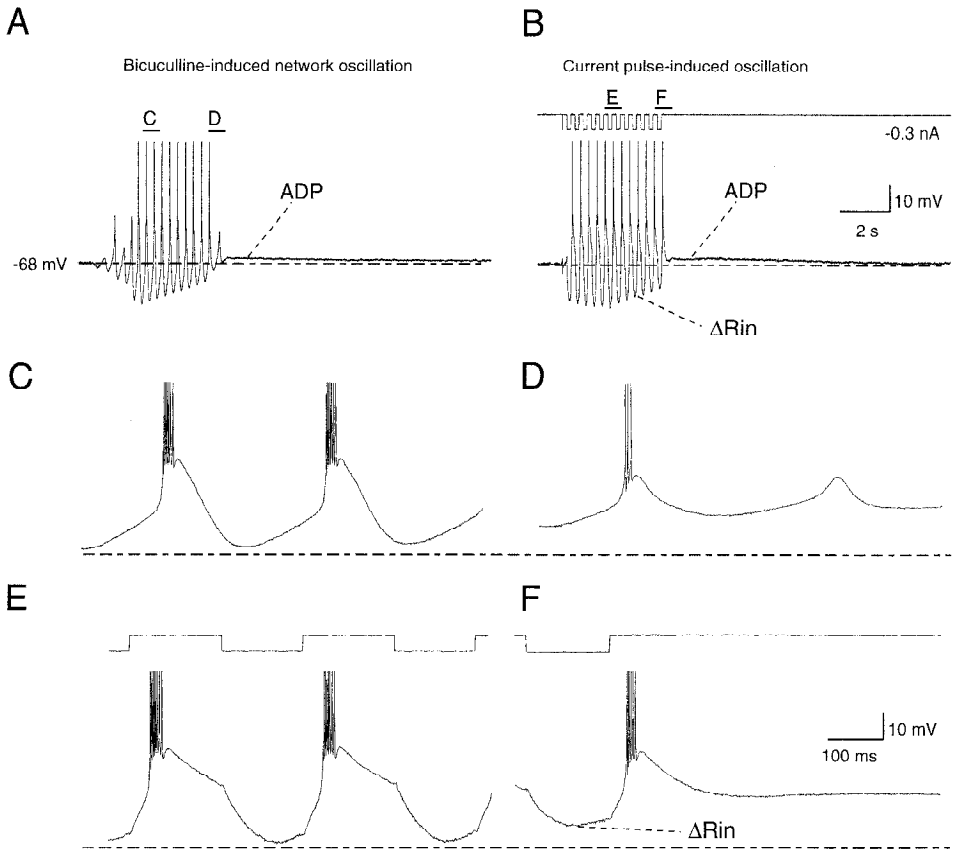


FIG. 4. TC cell bursts are followed by an afterdepolarization and diminished input resistance. *A*: afterdepolarization (ADP) after a spontaneously occurring oscillation in a cell from lateral geniculate nucleus in vitro. *B*: same cell, but a sequence of rebound bursts was induced by injecting hyperpolarizing current pulses at 3 Hz (current shown *top*). Examples of rebound bursts at beginning (*C*) and end (*D*) of spontaneous oscillation show that IPSPs have diminished effect on the cell and that bursts gradually become weaker. The same phenomenon is seen during injection of current pulses (*E* and *F*). During the sequence of injected pulses, there was a progressive decrease of input resistance ($\Delta Rin$).

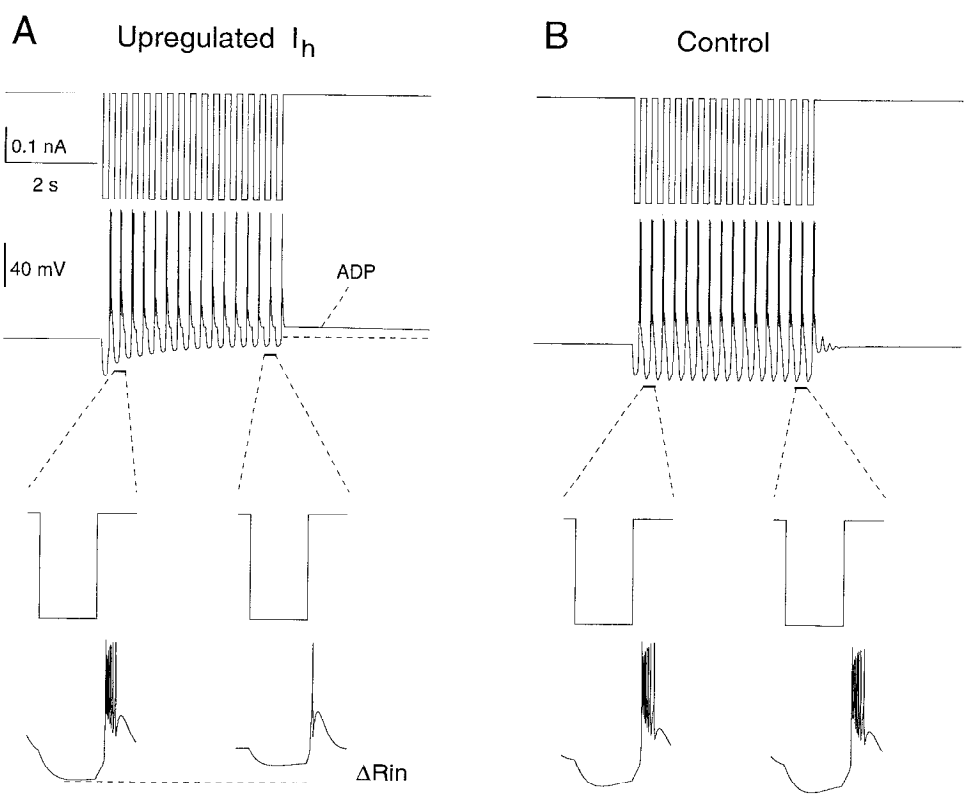


FIG. 5. Diminution of input resistance and ADP in model TC cells. Hyperpolarizing current pulses were injected at 4 Hz evoking a sequence of rebound bursts (injected current shown *top*). *A*: when there was an activity-dependent upregulation of $I_h$, voltage responses gradually decreased, indicating a diminution of input resistance ($\Delta Rin$, *insets*). Successive bursts became progressively less powerful. At the end of the sequence, membrane showed an ADP. *B*: without upregulation of $I_h$, none of these phenomena was present, although a stronger $I_h$ conductance was used. *Bottom*: enlargement of 2nd and 15th pulses and responses; $\bar{g}_h = 0.025$ mS/cm$^2$ $g_{KL} = 5$ nS in *A* and $\bar{g}_h = 0.08$ mS/cm$^2$, $g_{KL} = 5$ nS in *B*.

diminution of input resistance with a time constant of ~700 ms (Fig. 5*A*). This phenomenon did not occur using nonregulated $I_h$ even with a stronger $I_h$ (Fig. 5*B*). The ADP was present in both spontaneous oscillations (Fig. 3*B*) and after a sequence of rebound bursts evoked by current injection (Fig. 5*A*). The depolarization was caused by a progressive enhancement of the $I_h$ current.

From Figs. 4 and 5, it also is apparent that after a few bursts, there is a reduced tendency of the TC cell for further rebound burst responses. The progressive augmentation of the $I_h$ conductance depolarizes the membrane and counteracts the deinactivation of $I_T$, and weaker rebound responses follow. This phenomenon was not seen in the absence of upregulation of $I_h$ (Fig. 5*B*). This property will have important consequences at the network level, as shown in later sections.

When the model TC cell was stimulated by GABAergic synaptic currents, the response depended on the type of receptor, the conductance and the frequency of stimulation. Figure 6, *A* and *B*, shows repetitive stimulation of $GABA_A$ receptors at 10 Hz. Stimuli consisted of short bursts of presynaptic pulses occurring every 100 ms. These stimuli were insufficient to activate $GABA_B$ receptors, but activated $GABA_A$ IPSPs occurring at 10 Hz in the cell. For moderate to low $GABA_A$ conductances, the TC cell responded by producing rebound bursts once every two synaptic stimuli (Fig. 6*A*). This phenomenon of subharmonic bursting has been described before (Kopell and LeMasson 1994; Wang 1994) and is due to the presence of $I_T$ and $I_h$. Subharmonic bursting is consistently seen in TC cells during spindle oscillations in different preparations (Bal et al. 1995a,b; Muhlethaler and Serafin 1990; Steriade and Deschênes 1984).

For stronger $GABA_A$ conductances, the TC cell could produce rebound bursts at 10 Hz (Fig. 6*B*), similar to the results of a previous model (Destexhe et al. 1993b). During spindle oscillations, some types of TC cells typically burst on each cycle during spindle oscillations, as observed in thalamic intralaminar cells (Steriade et al. 1993a).

Stimulation of $GABA_B$ receptors at 3.3 Hz with long bursts of presynaptic pulses occurring every 300 ms and with $GABA_A$ receptors blocked produced very robust rebound bursts at the same frequency (Fig. 6*C*). These bursts were larger due to the more complete deinactivation of $I_T$ provided by $GABA_B$ IPSPs.

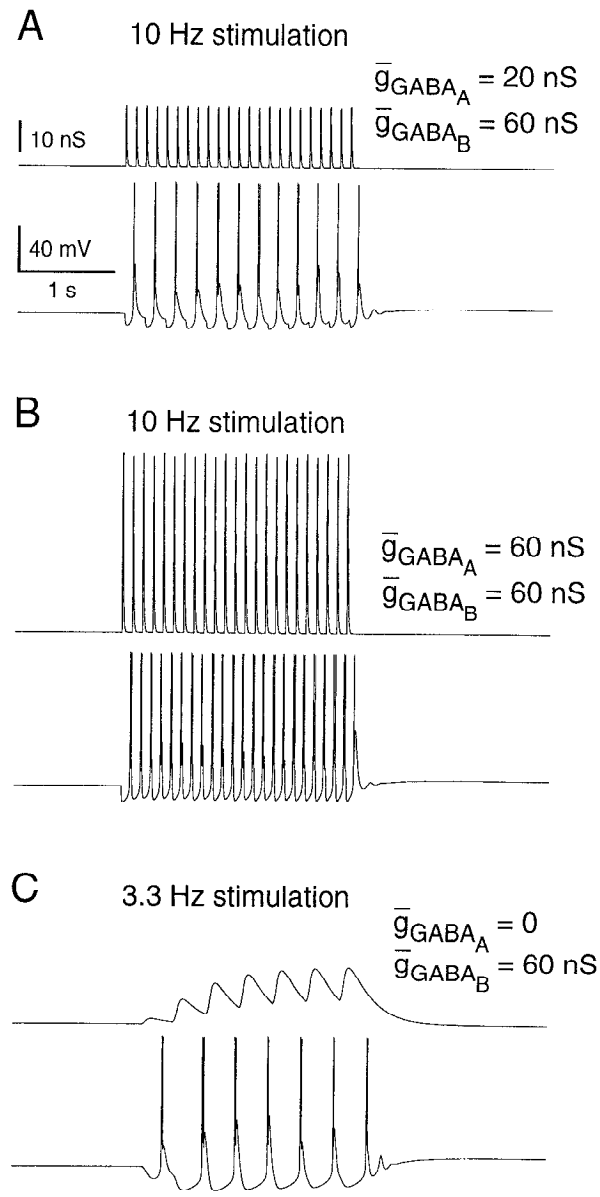


FIG. 6. Simulated responses of thalamocortical cells to GABAergic synaptic stimulation. Both $GABA_A$ and $GABA_B$ receptors were stimulated at either 10 or 3.3 Hz in a TC cell. Stimuli were bursts of presynaptic pulses at 360 Hz mimicking frequency of RE bursts (see Fig. 2, *A2* and *A3*). *A*: subharmonic response of TC cell to GABAergic stimulation at 10 Hz. GABAergic receptors were stimulated using bursts of 3 pulses at 360 Hz, occurring every 100 ms. $GABA_A$ conductance is represented (*top*) with membrane potential (*bottom*). TC cell produced rebound bursts at half of the stimulation frequency (5 Hz). *B*: same simulation, but using 3 times stronger $GABA_A$ conductance. In this case, the TC cell was recruited into bursting oscillations at 10 Hz. *C*: stimulation (3.3 Hz) of $GABA_B$ receptors alone ($GABA_B$ conductance is drawn on *top*). In this case, 7 successive bursts were simulated with an interburst period of 300 ms; each burst in the stimulus consisted of a train of 18 pulses at 360 Hz, mimicking the firing patterns of RE cells in absence of $GABA_A$ receptors (see Fig. 2*A3*). Contrary to stimuli in *A* and *B*, which evoked a weak $GABA_B$ component in the IPSP (see Fig. 2*A*), stimulus used in *C* evoked strong $GABA_B$-mediated currents and the TC cell was recruited in secure rebound bursts responses.

*Spindle oscillations from small circuits of thalamic cells*

We now turn to small systems of interconnected TC and RE cells, using $GABA_A$ receptor synapses between RE cells, AMPA receptor synapses from TC to RE cells, and a mixture of $GABA_A$ and $GABA_B$ receptors at inhibitory synapses from RE to TC cells, using the same kinetics as described above. In a previous model (Destexhe et al. 1993b), an interacting pair of TC and RE cells showed 9–11 Hz waxing-and-waning oscillations similar to spindle oscillations. However, to have a two-cell minimal model, the TC cell had to produce a rebound burst after each $GABA_A$ IPSP arriving at 10 Hz (as in Fig. 6*B*). The same type of oscillations could be found using the present models together with strong $GABA_A$ conductances (not shown). However, intracellular recordings of TC cells during spindling show subharmonic bursting with the TC cell producing rebound bursts every two or three GABAergic IPSPs, a feature that cannot be reproduced with only one TC cell.

In a previous model (Destexhe et al. 1993a), blocking all

GABAergic conductances did not lead to the cessation of oscillatory activity in the two-cell model because the TC cell needed to have spontaneous oscillatory activity: this may be relaxed in models of larger networks where there is a range of intrinsic properties among the TC cells (Leresche et al. 1991). One possible source of heterogeneity in the intrinsic properties of TC cells is a difference in their resting membrane potential, as would occur if they had different values of $I_h$ and leak $K^+$ conductances. Even if most TC cells are in a relay mode, with a depolarized resting membrane potential around −60 mV, some TC cells could oscillate spontaneously, due to a weaker $I_h$ maximal conductance. This is consistent with current-clamp recordings in TC cells in vitro (Leresche et al. 1991; McCormick and Pape 1990a; Soltesz et al. 1991), in which both resting and spontaneously oscillating TC cells were found. Such an inhomogeneity in the properties of TC cells may account for the initiation and propagation of spindle activity, as shown in the next section.

A minimal model for spindle activity that takes into account the properties described above has two TC and two RE cells, as shown in Fig. 7. In this circuit, the weaker $GABA_A$ conductances recruited the TC cell to rebound once every two IPSPs, alternating with each other, such that the RE cells received EPSPs occurring at ~10 Hz although each TC cell burst at ~5 Hz. The two TC cells in this model were different. There was an "initiator" TC cell (TC1 in Fig. 7), which had a stronger $I_h$ and was spontaneously oscillating, and a "follower" TC cell (TC2 in Fig. 7), which was in a resting relay state and had weaker $I_h$. TC1 began oscillating and recruited the two RE cells, which in turn recruited TC2. The oscillation in the whole system was maintained at a frequency of 9–11 Hz during the spindle. After a few cycles, the $Ca^{2+}$-induced augmentation of $I_h$ conductance depolarized the membrane in both TC cells and the oscillation stopped. After a silent period of 15–25 s, the initiator TC cell began to oscillate again and the cycle repeated.

During the spindle oscillation, there was a mirror image between bursts in the TC and RE cells that is typical of those observed from recordings (Fig. 7*B*). Bursts in the TC cell were rebound responses to IPSPs, and the oscillation rode on a hyperpolarizing envelope. In RE cells, EPSPs from TC cells activated $I_T$ and elicited bursts, leading to a depolarizing envelope during the spindle. This mirror image is characteristic of spindle oscillations recorded intracellularly in the two thalamic cells types (Bal et al., 1995a,b; Steriade and Llinás 1988; von Krosigk et al. 1993).

In this model, the rhythmicity was induced by the initiator TC cell, TC1, in an otherwise quiescent circuit. The oscillation also could be started by extrinsic mechanisms, such as by stimulating any TC or RE cell in the system (not shown). The resting TC cell, TC2, acted here as a conditional oscillator; although it did not oscillate spontaneously, $I_T$ and $I_h$ still were present in the cell, and it was able to participate in oscillatory behavior.

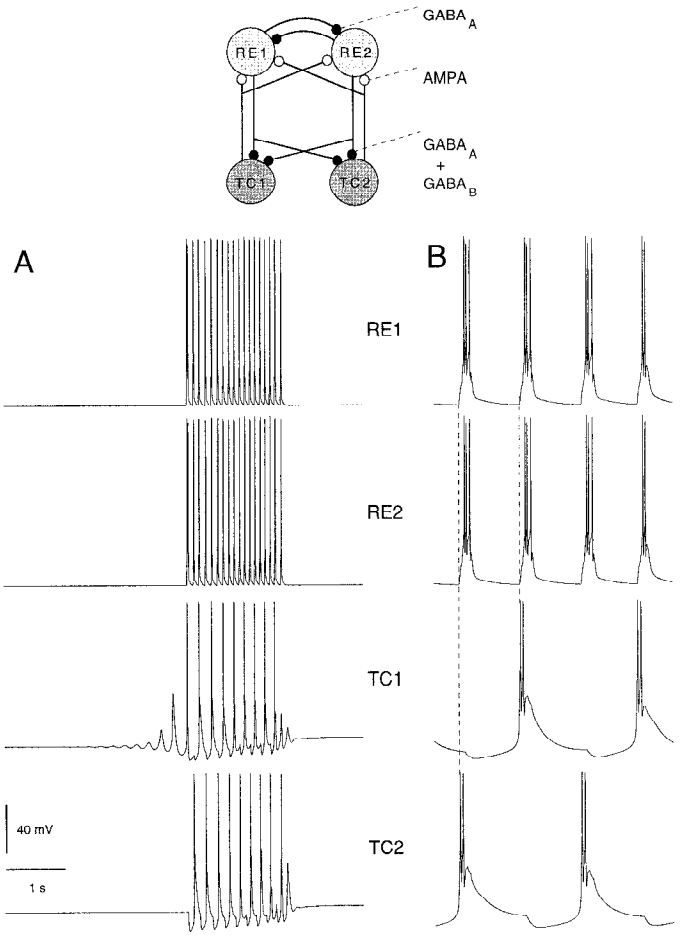


FIG. 7. Spindle oscillations in a 4-neuron circuit of thalamocortical and thalamic reticular cells. Two TC and 2 RE cells were connected as shown in diagrams above. One TC cell (TC1) was spontaneously oscillating (initiator cell) and had a higher conductance of $I_h$ ($\bar{g}_h$ = 0.025 mS/cm$^2$; $\bar{g}_{KL}$ = 5 nS). The second TC cell (TC2) had weaker $I_h$ and $g_{KL}$ ($\bar{g}_h$ = 0.015 mS/cm$^2$; $g_{KL}$ = 3 nS) and was in a resting mode. Two RE cells were identical. Synaptic currents were mediated by AMPA/kainate receptors (from TC to RE; $g_{AMPA}$ = 0.2 $\mu$S), a mixture of $GABA_A$ and $GABA_B$ receptors (from RE to TC; $g_{GABA_A}$ = 0.02 $\mu$S and $g_{GABA_B}$ = 0.04 $\mu$S) and $GABA_A$-mediated lateral inhibition between RE cells ($g_{GABA_A}$ = 0.2 $\mu$S). *A*: spindle oscillations arose as the 1st TC cell (TC1) started to oscillate, recruiting the 2 RE cells, which in turn recruited the 2nd TC cell. Oscillation was maintained for a few cycles and repeated with silent periods of 15–25 s. *B*: 1st bursts of same cells shown at 10 times higher time resolution. Each TC cell produced bursts at ~5 Hz, out of phase, but provided a common input at 9–11 Hz to RE cells. A burst in a TC cell always preceded bursts in RE cells by a few milliseconds.

*Bicuculline-induced oscillations*

In ferret thalamic slices, block of $GABA_A$ receptors by application of bicuculline transformed the spindle behavior into a slower (3–4 Hz) oscillation of high synchrony (Bal et al. 1995a; Kim et al. 1995; von Krosigk et al. 1993). Further application of a $GABA_B$ receptor antagonist abolished these slowed oscillations, indicating that their genesis involved $GABA_B$-receptor mediated IPSPs.

In the four-cell circuit, we observed a similar type of slow oscillation (Fig. 8). These oscillations were a consequence of the properties of $GABA_B$ responses as described above. After removal of $GABA_A$-mediated inhibition, the RE cells could produce prolonged bursts that evoked strong $GABA_B$ currents in TC cells (as described in Fig. 2*A3*). These prolonged IPSPs evoked robust rebound bursts in TC cells (as in Fig. 6*C*), and TC bursts in turn elicited bursting in RE cells through EPSPs. This mutual TC–RE interactions recruited the system into a 3- to 4-Hz slow oscillation with characteristics similar to those of

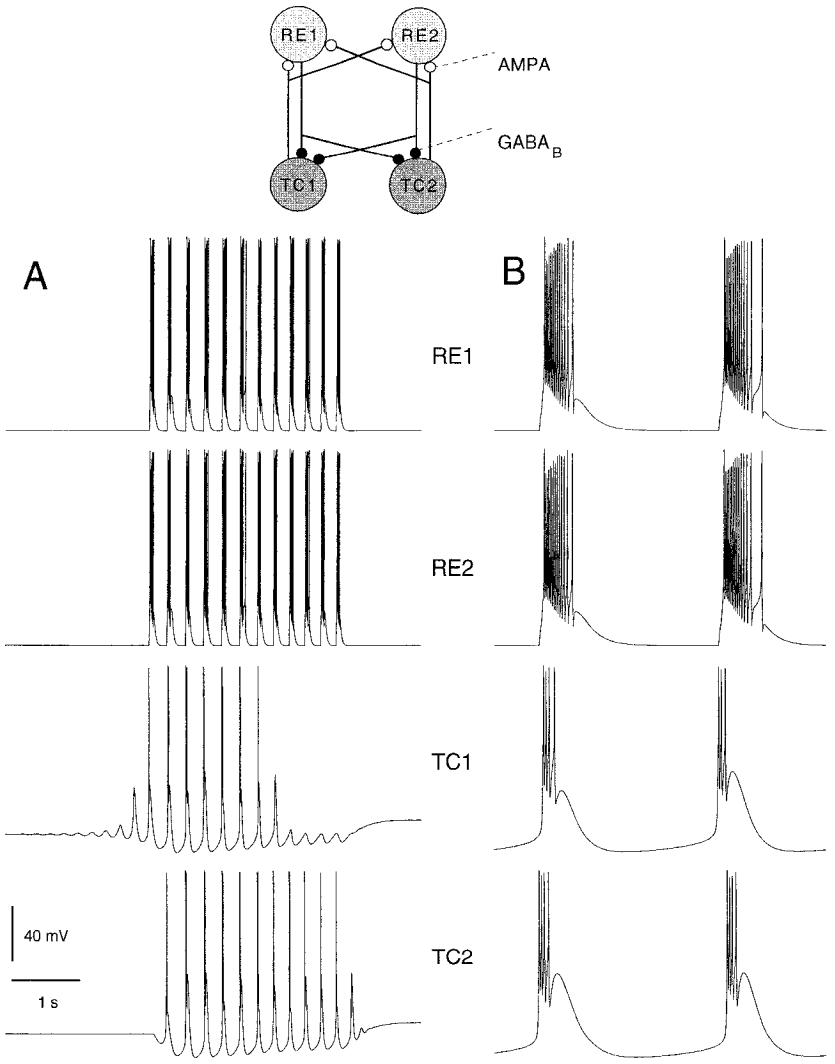


FIG. 8. Bicuculline-induced oscillations in a 4-neuron circuit of thalamocortical and thalamic reticular cells. The same circuit as described in Fig. 7 was used, but $GABA_A$ receptors were suppressed, mimicking effect of bicuculline. *A*: slow 3–4 Hz oscillation obtained as the 1st TC cell (TC1) started to oscillate, recruiting the 2 RE cells, which in turn recruited the 2nd TC cell. The mechanism of recruitment between cells was identical as for spindle oscillations (Fig. 7), but oscillations were more synchronized, of slower frequency, and had a 15% longer silent period. Burst discharges were prolonged due to loss of lateral inhibition in RE. *B*: first bursts of the same cells shown at 10 times higher time resolution. TC cells were in phase and phase-led RE cells by a few milliseconds.

bicuculline-induced slow oscillations in ferret thalamic slices. The oscillation was caused by the same mechanisms described in the previous section for spindle oscillations but was slower and more synchronized (Fig. 8).

In the model, the silent period of the oscillation was significantly longer for bicuculline-induced oscillations (26 ± 5 s, mean ± SD) compared with spindle waves (20 ± 6 s). The length of the silent period was sensitive to the maximal conductance of $I_h$ and the unbinding rate of calcium-binding protein from $I_h$ channels ($k_4$ in *Eq. 8*). For a given set of parameters, the period of bicuculline-induced oscillations was always longer than the period of spindles. This was observed consistently experimentally (Kim et al. 1995) but the difference was less pronounced in the model. We could match more closely the relative duration of the silent period with other parameter values, but the results were highly variable and not robust to small changes in the parameters. This sensitivity may be reflected in the variability that has been reported between experiments (Kim et al. 1995). The mechanism underlying longer interspindle periods was the stronger upregulation of $I_h$, as also shown by the higher amplitude of the ADP in the case of bicuculline-induced oscillations (see below).

In vitro experiments show that blocking TC-RE synaptic interconnections suppresses oscillatory behavior in both TC and RE cells (Bal et al. 1995a,b; von Krosigk et al. 1993). The present model is compatible with this result if resting TC cells are typical of the majority of the TC population. After blocking all synaptic receptors, only the few spontaneously oscillating TC cells will continue to oscillate, but all other TC cells and RE cells will remain silent, as shown in the next section.

### *Oscillations in networks of TC and RE cells*

The model of interaction between two TC cells and two RE cells was scaled up to larger networks. In Fig. 9, a model with 50 TC and 50 RE cells is shown having the same types of cells and synaptic receptors as in Fig. 7. Based on anatomic data showing that axonal projections in the thalamic circuitry are local and topographic (Fitzgibbon et al. 1995; Gonzalo-Ruiz and Lieberman 1995; Jones 1985; Minderhoud 1971; Sanderson 1971), we have approximated the structure of ferret thalamic slices by a two-layer one-dimensional network, one layer of TC cells and one layer of RE cells, in which connections were topo-

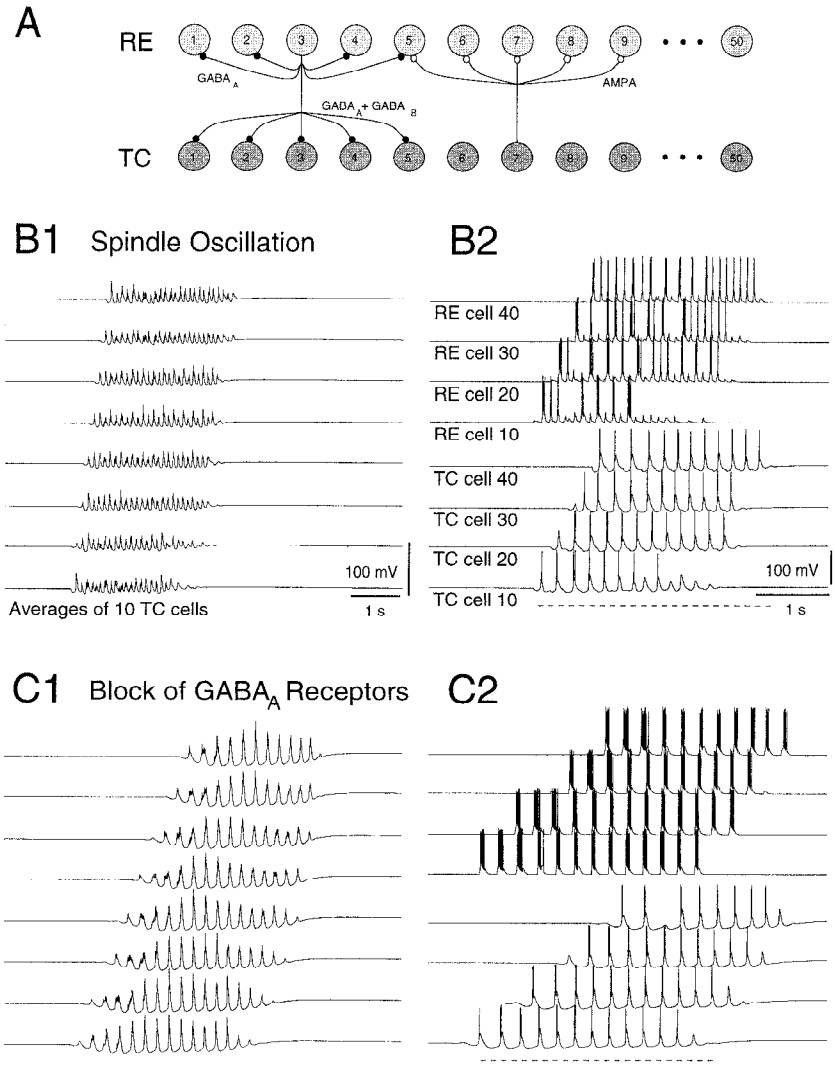


FIG. 9. Propagating oscillations in a network of thalamocortical and thalamic reticular cells. *A*: schematic diagram of connectivity of a 1-dimensional network of 50 TC and 50 RE cells with localized axonal projections. Axons from TC cells ramified in RE nucleus and contacted RE cells within a patch of 10% of the size of network. Similarly, axons from RE cells contacted TC cells as well as had collaterals within the RE nucleus. All projections extended laterally to 11 neurons in case shown here. TC1 was a spontaneously oscillating cell, whereas all other TC cells were in a resting mode; all RE cells were identical (same models as in Fig. 7). *B1*: spindle oscillations at various sites of network. Averaged membrane potentials were computed from 10 neighboring TC cells taken at 8 equally spaced sites. *B2*: membrane potential of 4 TC (4 *bottom traces*) and 4 RE cells (*top* traces) in the same simulation as in *B1*. *C1*: average membrane potentials of slow bicuculline-induced oscillations following removal of $GABA_A$ receptors. *C2*: example of TC and RE cells during the same simulation as in *C1*. (*C1* and *C2*: same sites and cells as in *B1* and *B2*.)

graphically local (Fig. 9*A*). Each cell type made axonal projections that contacted 11 neighboring cells in the other layer (and also within the same layer for RE cells). All axonal projections were identical in extent and all synaptic conductances were equal. The total synaptic conductance on each neuron was the same for cells of the same type, independently of the size of the network, and was also the same as cells in the four-cell circuit. Reflexive boundary conditions were used to minimize boundary effects (see Destexhe et al. 1994a).

Averaged membrane potentials over local regions of 10 cells, regularly spaced throughout the network, showed waxing-and-waning oscillations at ~10 Hz, indicating that the cells oscillated in synchrony (Fig. 9*B1*). As in the four-cell circuit, TC cells oscillated at a slower frequency ~5 Hz whereas RE cells tended to oscillate ~10 Hz but had more irregular behavior (Fig. 9*B2*).

In individual cells, the oscillation showed waxing-and-waning properties similar to those described above (Fig. 9*B2*). The waxing oscillation propagated as more and more cells were recruited. Similarly, the waning also propagated, as TC cells progressively lost their ability to participate in rebound bursting activity. The resulting pattern had the appearance of waves of oscillatory activity propagating through the network. Between waves, the network was quiescent for 15–25 s.

The presence of propagating waves in the 100-cell network depended on the restricted topographic connectivity between the TC and RE layers. With topographic connectivity, the oscillation started at one site, and always propagated through the involvement of more TC and RE cells recruited at each cycle of the oscillation. The velocity of the propagation was directly proportional to the extent of the axonal projections, similar to what was reported in a previous study (Golomb et al. 1996). Similar results were found with different sets of parameters so long as the connectivity was restricted topographically (not shown).

The phase relationships between TC and RE cells can be used to assess causal relationships. In Figs. 7 and 9, the initiator TC cell (TC1) started oscillating first and recruited RE cells. However, the other TC cells always started spindling with an IPSP and followed the RE cells. If now these follower TC cells constituted the majority of the TC population, then comparing RE cells with this type of TC cell could lead to the misleading interpretation that RE cells start spindle oscillations. The model therefore suggests that, even

if the overwhelming majority of TC cells start spindles with IPSPs, the spindle sequence still can be initiated by a small minority of TC cells.

Bicuculline-induced oscillations also supported propagating-wave phenomena when the connectivity between the TC and RE layers was restricted (Fig. 9*C*). In this case, the synchrony was significantly higher inside the oscillatory sequence, as shown by the amplitude of averaged activities (Fig. 9*C1*) and by comparing individual membrane potential traces across the network (Fig. 9*C2*). This increase of synchrony was confirmed by cross-correlation analysis (Fig. 10). In addition, there was a progressive phase shift that increased with the distance between sites, seen as a the time shift of the maximum correlation in Fig. 10, *A* and *B*. The higher synchrony for bicuculline oscillations and the progressive phase shifts have been observed in ferret thalamic slices (Kim et al. 1995).

Correlations show a progressive decay with distance, with a rate of decay that is similar for both types of oscillations (Fig. 10*C*), as expected for propagating oscillations. For all parameter values and connectivity tested, the propagation velocity for bicuculline-induced oscillations was slower than for spindle oscillations, which also was observed consistently in ferret thalamic slices (Kim et al. 1995). The average propagation delay between two neighboring neurons was of ~19.4 ms for spindles and 55 ms for bicuculline-induced oscillations. If we assume that the fan-out of the projections between the TC and RE cells in the model (11 neurons) is equivalent to 200 $\mu$m in the slice, then the velocity in the model is ~1.03 mm/s for spindles, which is within the range 0.28 to 1.21 mm/s observed experimentally, and the velocity for bicuculline-induced oscillations was 0.36 mm/s, compared with the range 0.22–0.95 mm/s observed experimentally. Although these values approximately match, the model systematically produced a larger difference between the spindle velocity and the bicuculline-induced oscillation velocity than observed experimentally, presumably due to the small size of the network and the homogeneous patterns of connectivity that we used (see also Golomb et al. 1996).

Intracellular recordings from TC cells in ferret thalamic slices revealed a prominent ADP occurring in the inter-spindle silent period (Fig. 11*A*, *top*). This ADP was more prominent during bicuculline-induced slow oscillations (Fig. 11*A*, *bottom*). The same phenomenon occurred in the model (Fig. 11*B*) and was due to upregulation of $I_h$. The increased ADP during bicuculline-induced oscillations also was displayed in the model (Fig. 11*B*, *bottom*) and was due to the stronger activation of $I_T$ underlying prolonged burst discharges, leading to more calcium entry and a more pronounced upregulation of $I_h$.

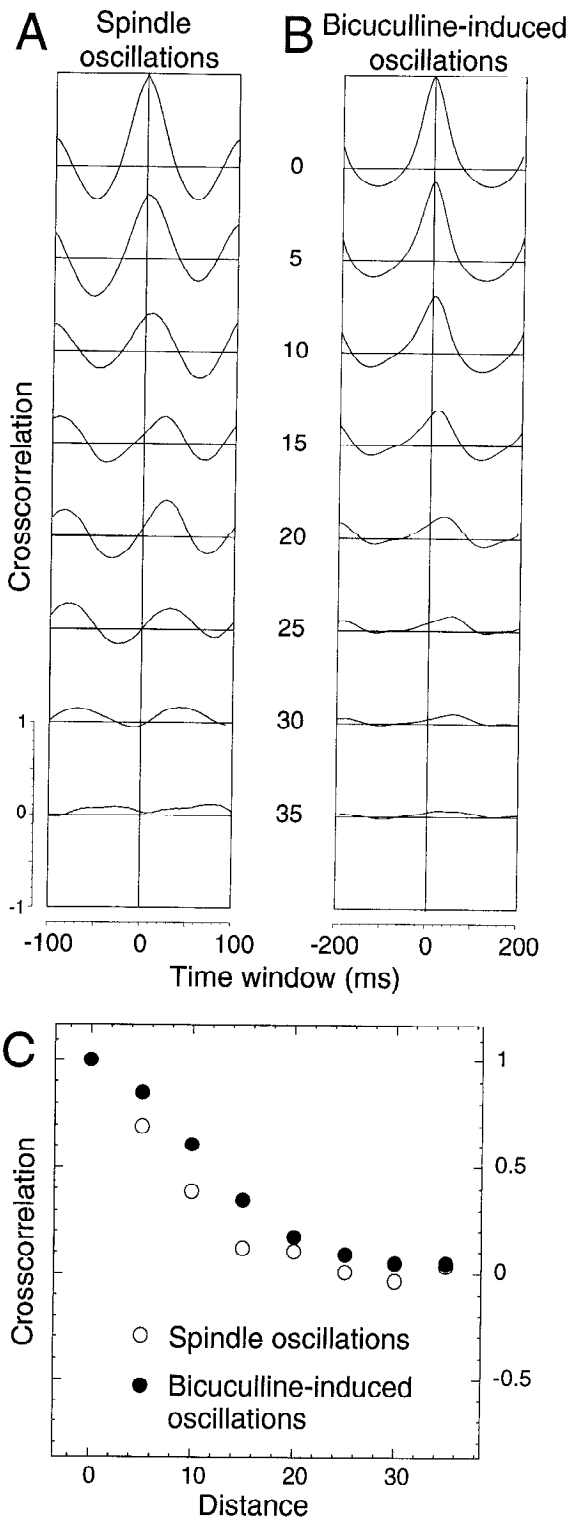


FIG. 10. Cross-correlations between different sites during spindle waves and bicuculline-induced oscillations. Correlations were evaluated between a reference site (TC cell 10) and sites taken at progressively larger distances (units of intercellular distances in the network; intersite distance shown for each graph). *A*: cross-correlations during spindle oscillations. *B*: cross-correlations during bicuculline-induced oscillations. In both cases, the correlation was calculated between averages of TC cells (same simulation and averaging procedures as in Fig. 9). *C*: space correlation calculated as the cross-correlation at *time 0*, plotted as a function of distance between sites. For both oscillations, correlations decayed with distance, but bicuculline-induced oscillations were always of higher correlation than spindles and are therefore more synchronized.

### *Spatiotemporal patterns of discharges*

For spindle waves, the spatiotemporal patterns of discharges, shown in Fig. 12, had the following properties: first, the waxing and the waning of the oscillation had a similar velocity. Second, during the oscillation, groups of cells segregated into localized clusters of activity, discharging in alternation. This phenomenon is associated with the subharmonic bursting properties of TC cells, which does not allow the whole network to fire in unison at ~10 Hz. Third, indi-

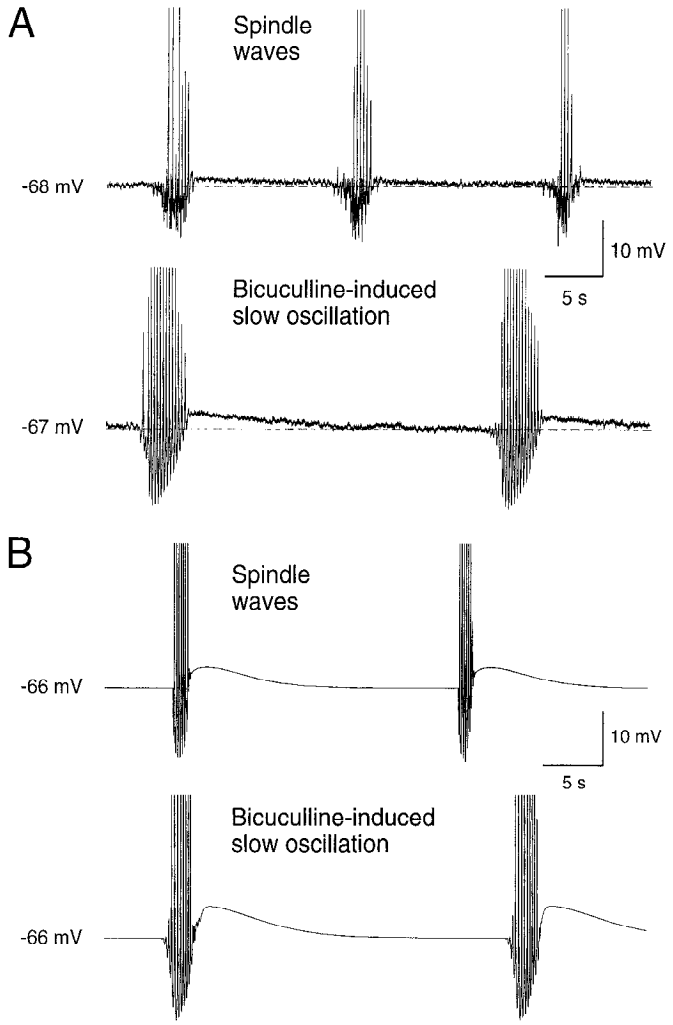


FIG. 11. ADP in TC cells during spindle and bicuculline-induced oscillations. *A*: comparison of spindle and bicuculline-induced oscillations in an intracellularly recorded TC cell in ferret thalamic slices. Before (*top*) and after (*bottom*) application of bicuculline, the silent period between oscillations showed an ADP that was more prominent during bicuculline-induced oscillations. *B*: same oscillations simulated using a network of 50 TC and 50 RE cells (from Fig. 9), in normal conditions (*top*) and after block of $GABA_A$ receptors (*bottom*). In this case, the ADP occurred in all TC cells of the network due to upregulation of $I_h$. A more pronounced enhancement of $I_h$ was responsible for the larger ADP in bicuculline-induced oscillations. Sodium spikes were truncated in all traces.

vidual clusters of activity also propagated with the same velocity as the whole oscillation. This phenomenon can be seen most clearly when the snapshots are played as a movie.[1] The simulated spindles appear to be composed of a series of successive clusters of activity that follow each other and propagate through the TC-RE structure. The cluster of activity at the front of the propagating oscillation can be seen clearly in the top series of frames in Fig. 12.

The only inhomogeneity in the 100-cell network was the first TC cell, which had a higher $I_h$ conductance and was spontaneously oscillating, as in the four-cell circuit; all RE cells were identical. The presence of only one oscillating TC cell was sufficient to initiate a spindle oscillation in the whole network. The recruitment mechanism is illustrated in Fig. 12 (*inset*). The initiator TC cell (TC1) discharged first due to intrinsic oscillatory properties (arrow 1 in Fig. 12). AMPA-mediated EPSPs were evoked in neighboring RE cells (arrow 2) following the discharge of TC1; these EPSPs were strong enough to activate $I_T$ and evoke burst firing in RE cells (arrow 3). RE cell bursts then recruited neighboring TC cells though GABAergic IPSPs (arrow 4). Following this inhibition, some TC cells produced rebound bursts (arrow 5) due to deinactivation of $I_T$, and the same sequence restarted. This back-and-forth series of interactions between cells in the TC and the RE layers recruited additional cells into the spindle oscillation on every cycle. After a few cycles, the $Ca^{2+}$-induced augmentation of $I_h$ conductance in TC cells stopped the oscillation. After a silent period of 15–25 s, the initiator TC cell began to oscillate again and the cycle repeated.

The spatiotemporal pattern of activity dramatically changes when $GABA_A$-mediated currents are suppressed (Fig. 13). In this case, the waxing and the waning of the bicuculline-induced oscillation both propagated with a lower velocity compared with spindles. The bursts were not organized in distinct clusters but instead involved a much larger population of cells with more prolonged discharges (compare Fig. 12 with Fig. 13). In this sense, the oscillation was more synchronized. However, bursting discharges did not appear simultaneously in the whole network but rather started at a focus and invaded the network progressively, leading to curved patterns in the successive snapshots (Fig. 13). This phase shift also was observed in other instances of these oscillations (not shown) and had no preferential direction.

### *Refractoriness of the network*

The upregulation of $I_h$, leading to a diminished tendency of TC cells to sustain rebound bursts immediately after an oscillatory sequence, underlies the waning of spindle oscillations. Upregulation of $I_h$ also has other consequences at the network level, such as the noncrossing of colliding waves, the presence of refractoriness in the network, and sustained oscillations if $I_h$ is altered. These conditions are examined successively in this section.

In ferret thalamic slices (Kim et al. 1995), two spindle waves propagating in opposite directions will not cross, but rather merge into a unique oscillation. This also is observed in the model because of the refractoriness of the cells (Fig. 14*A*). Two spindle waves, initiated from the opposite edges of the network with a 50-ms delay to produce out-of-phase oscillations, propagated into the center and collided. Upon collision, the two waves became synchronous (compare dashed lines before and after collision in Fig. 14*A*). The waves did not cross due to upregulation of $I_h$ in TC cells and the consequent refractoriness was imparted to the network.

The refractoriness of thalamic networks have been shown explicitly in ferret slices experiments (Kim et al. 1995), as well as in cortical stimulation in cats in vivo (D. Contreras, A. Destexhe, T. J. Sejnowski, and M. Steriade, unpublished observations). In these experiments, oscillations evoked by electrical stimulation depended sensitively on the timing of

[1] Movie files (mpeg format) showing the propagating wave activity in the model are available on request or may be retrieved from internet (http://www.cnl.salk.edu/~alain/).

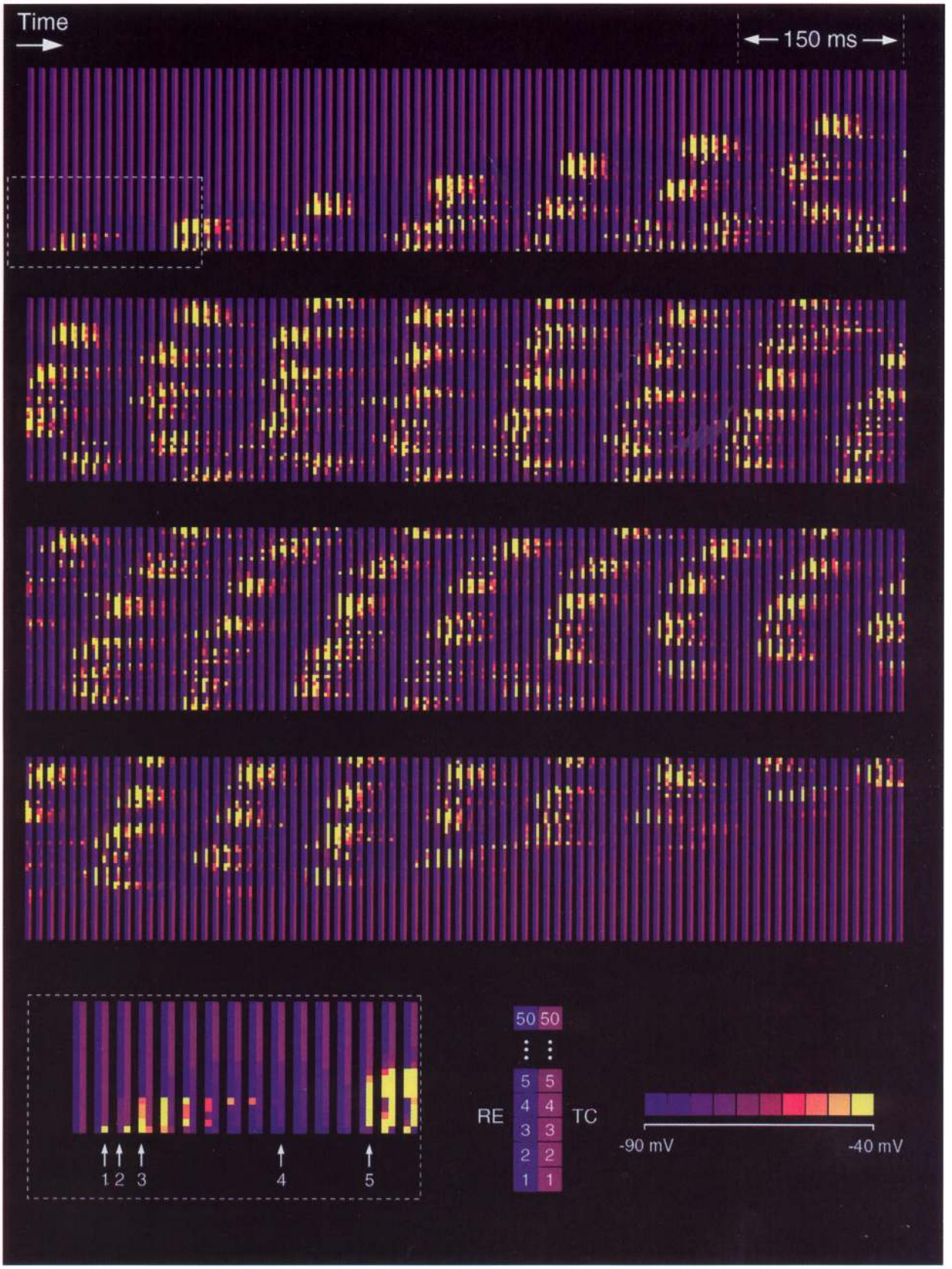


FIG. 12. Spatial patterns of burst discharges during spindle oscillations. The spatial activity of the network is represented as a series of snapshots of activity. A series of successive frames is shown for an entire spindle sequence (320 frames with 10 ms between frames; sequence indicated by a dashed line in Fig. 9*B2*). The activity consisted in a series of distinct clusters of activity propagating in same direction. Initiation of spindle sequence is expanded, *bottom left*. For each snapshot, 50 TC and 50 RE cells were displayed vertically as indicated (*middle scheme at bottom*). The value of the membrane potential for each neuron was coded using a color scale ranging in 10 steps from −90 mV (blue) to −40 mV (yellow).

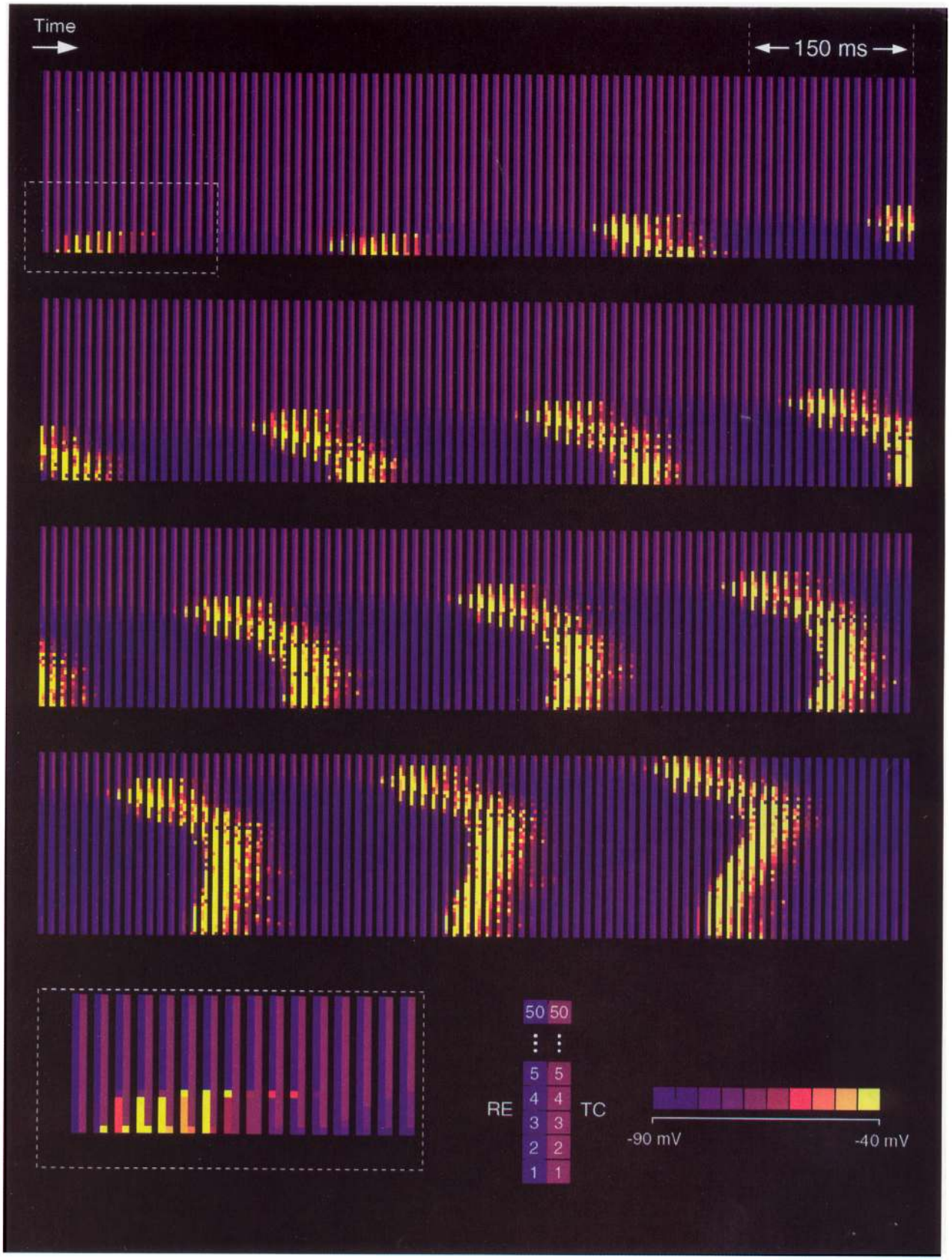


FIG. 13. Spatiotemporal patterns of discharges during bicuculline-induced oscillations. Same description as Fig. 12 but from the simulation shown in Fig. 9*C*. Unlike spindles, bicuculline-induced oscillations are characterized by a more uniform pattern of discharge that propagates with a slower velocity.

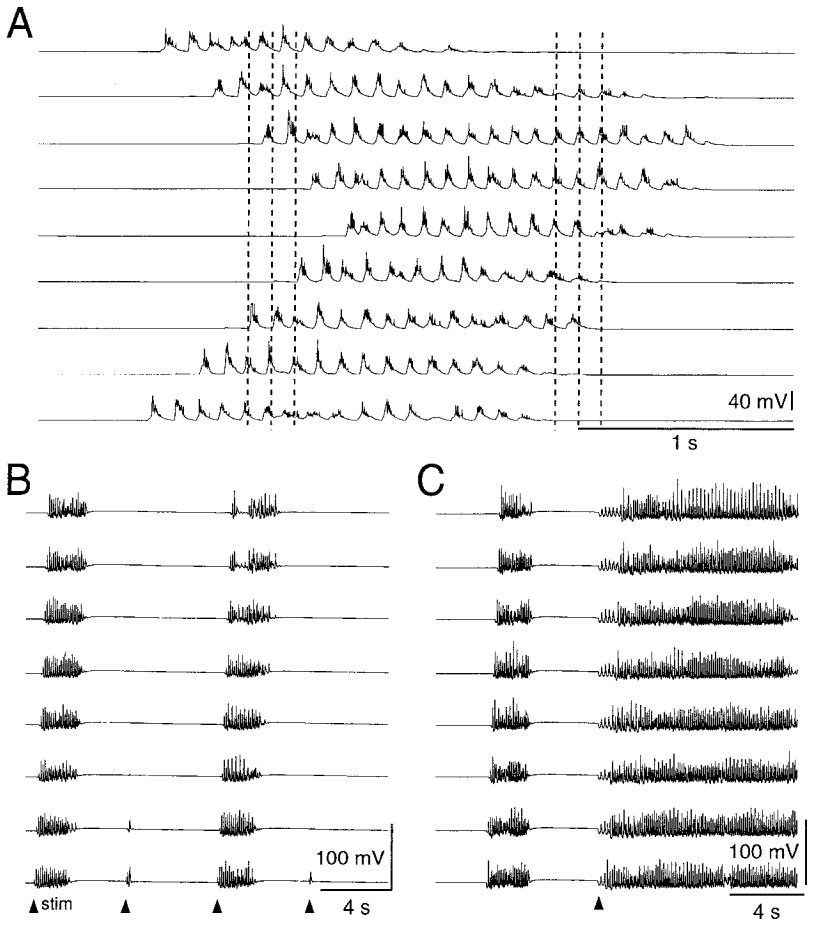


FIG. 14. Network properties of propagating spindle oscillations. *A*: collision between 2 simulated spindle waves. Three TC cells at each edge of network were stimulated by depolarizing current pulses (1 nA during 40 ms). One stimulation preceded the other by 50 ms to produce spindles that were initially out of phase (1st series of dashed lines). Two waves collided without crossing each other, and came into synchrony (dashed lines on the *left*). The network was of 100 TC and 100 RE cells with identical connectivity and parameters as in Fig. 9*A*. *B*: refractoriness of spindle oscillations. Repetitive stimulation was delivered on 3 TC cells at 1 edge of network. Depolarizing current pulses of 1 nA during 40 ms were delivered every 5 s (arrows). Stimulations occurring 10 s after a spindle sequence successfully evoked propagating spindle oscillations, but those occurring after 5 s failed to evoke propagating oscillations. *C*: transformation from spindle oscillations to sustained oscillations by reducing $I_h$ conductances. In all TC cells the maximal conductance was set to 0.004 mS/cm$^2$ (arrow), mimicking extracellular application of cesium. Spontaneous waxing-and-waning spindles (before arrow) were transformed into sustained rhythmicity with similar frequency and cellular behavior as spindles. *A–C* were with identical parameters and averaging procedures as in Fig. 9*B*.

the stimulus relative to the previous spindle sequence. This dependency also was present in the model, as illustrated in Fig. 14*B*. After a spindle sequence, there was a refractory period of ~8–10 s during which no propagating oscillations could be evoked. This phenomenon is therefore consistent with an activity-dependent upregulation of $I_h$. After a spindle sequence, activation of $I_h$ was increased to the point that TC cells were unable to sustain further oscillations, which lasted until $I_h$ slowly recovered to its resting level.

In ferret thalamic slices (Kim et al. 1995), the refractory period was always shorter than the period for spontaneous oscillations. This was also true in the model, as shown for example by comparing Fig. 11*B* (*top*) with Fig. 14*B*, which had the same parameters. In the model, the network recovered full excitability after ~8–10 s whereas the spontaneous interspindle period was of the order of 20 s. This property was due to the spontaneously oscillating initiator TC cells that imprinted their oscillation period to the whole network. At any time between ~10 s after a spindle sequence and the next spindle sequence, a propagating oscillation could be initiated in the network by stimulation of either TC or RE cells.

Finally, in recent experiments, extracellular cesium transformed waxing-and-waning spindles into sustained rhythmicity at the same frequency (Bal and McCormick 1996). As extracellular cesium primarily affects $I_h$, these experiments suggest that $I_h$ plays a central role in waxing-and-waning processes. This is also consistent with the present model as shown in Fig. 14*C*. Reducing $I_h$ to a fraction of its initial conductance led to sustained oscillations of ~9 Hz. In this case, although the remaining $I_h$ still was upregulated by intracellular $Ca^{2+}$, it was not strong enough to suppress the rebound burst properties in TC neurons and consequently the oscillations remained sustained.

## DISCUSSION

Spindle rhythmicity is a well-established phenomenon that has proven to be favorable for exploring the relationship between the properties of single neurons and those of networks of neurons (Steriade et al. 1993b). Intracellular recordings of thalamic cells in vivo and in vitro have revealed that the membrane potential of TC cells ride on a hyperpolarizing envelope, with rebound bursts produced after IPSPs from RE cells. In comparison, TC cells evoke bursts in RE cells through EPSPs, producing a "mirror image" between the two types of cells (Steriade and Llinás 1988; von Krosigk et al. 1993). These findings are consistent with the hypothesis that the recruitment of TC and RE neurons is the basis of spindle rhythms. It is, however, difficult to confirm conclusively this hypothesis given the complexity of the system.

Computational studies have been used to explore the mechanisms of thalamic rhythmicity starting with the seminal model introduced by Andersen and Rutjord (1964), who predicted the importance of rebound bursts. Several models of spindle rhythmicity have been proposed recently for the

isolated reticular nucleus (Destexhe et al. 1994a; Golomb et al. 1994) as well as for the bidirectional interaction between TC and RE cells (Destexhe et al. 1993b; Golomb et al. 1996). Without firm ties to experimental measurements, however, these models are difficult to verify. By using computational models based on physiological and biophysical data, it has been possible to generate plausible hypotheses and decisive predictions to test them. We have shown here how experimental data from different preparations, sometimes with apparently contrasting results, can be reconciled and used to illuminate different facets of the same framework.

### *Components of spindle oscillations*

The intrinsic properties of TC cells are fundamental to several types of activity, including tonic firing, spindle oscillations, and delta oscillations, as well as epileptic discharges (see Steriade et al. 1993b). In slices, TC cells can generate intrinsic delta oscillations (Leresche et al. 1991; McCormick and Pape 1990a) with subpopulations of these neurons exhibiting intrinsic waxing-and-waning patterns (Leresche et al. 1991). The occurrence of these resting and oscillatory states depends on the membrane potential and the regulation of $I_h$ by several neuromodulators, such as noradrenaline and serotonin (McCormick and Pape 1990a; Soltesz et al. 1991). In the present model, the TC cell could display all these patterns at the same membrane potential but with different values of $I_h$ conductance (see Fig. 3), consistent with the hypothesis of Soltesz et al. (1991).

Unlike TC cells, RE cells do not generate sustained oscillations intrinsically, but GABAergic interactions between them can produce oscillations (Destexhe et al. 1994a; Golomb et al. 1994) in a manner that depends sensitively on the membrane potential (Destexhe et al. 1994b). This latter property could explain why the isolated RE nucleus displays oscillations in vivo (Steriade et al. 1987), but not in slices (Bal and McCormick 1993; Huguenard and Prince 1994b; von Krosigk et al. 1993; Warren et al. 1994). In the present model, the thalamic RE nucleus exhibited an oscillatory state or a quiescent state depending on the resting level of RE cells and the level of ascending neuromodulation (Fig. 2*C*) (see also Destexhe et al. 1994b).

The present model shows that quiescent TC and RE cells endowed with such properties and interconnected with excitatory and inhibitory connections can generate oscillations in the spindle range, in agreement with previous models (Destexhe et al. 1993b; Golomb et al. 1996). If connections between TC and RE cells in either direction are suppressed in the ferret slice preparation, the ability of the network to generate spindle oscillations is lost (Bal et al. 1995a,b; von Krosigk et al. 1993).

During spindles, TC cells discharged bursts only once every few cycles of the oscillation, a typical feature of spindle rhythmicity (Bal et al. 1995a,b; Muhlethaler and Serafin 1990; Steriade and Llinás 1988). However, we found that this pattern of bursting depended highly on the conductances of the intrinsic currents and on $GABA_A$-mediated IPSPs: strong conductances would recruit the TC bursts at every cycle of the oscillation, as in a previous model (Destexhe et al. 1993b). Similar features have been observed in intracellular recordings of thalamic intralaminar cells in vivo (Steriade et al. 1993a), suggesting that $GABA_A$ IPSPs from RE cells might be stronger in intralaminar TC cells. Alternatively, $I_T$ in these cells might have faster kinetics for the removal of inactivation or there may be another outward current that would help the cell in removing $I_T$ inactivation and in generating faster rebound.

### *Initiation, propagation, and termination of spindle oscillations*

Even assuming that the above description of spindle wave generation is correct, many questions remain concerning the initiation, propagation, and termination of these oscillations.

HOW IS A SPINDLE INITIATED? Spindle waves have been observed in the thalamus in the absence of cortical or prethalamic inputs (Morison and Bassett 1945). Several hypotheses have been proposed for the initiation of a spindle sequence. First, a region of the thalamus might be more excitable and spontaneous firing could start an oscillation (Kim et al. 1995). This is supported by a report that stimulation of a single RE cell could initiate a spindle wave in thalamic slices (Kim et al. 1995). Second, there could be spontaneously oscillating TC cells in an otherwise homogeneous network that would recruit the whole network into spindle rhythmicity. We have explored here the latter hypothesis in our model.

If a small minority of TC cells displayed spontaneous oscillations, they were able to recruit the rest of the network into spindle oscillations. Only a single initiator TC was needed in small networks of around a hundred cells. Blocking either excitatory or inhibitory transmission resulted in a quiescent network, as observed experimentally (von Krosigk et al. 1993). If several TC cells are needed to discharge one RE cell, then the spindle is initiated when burst discharges occur in several TC cells simultaneously "by chance" and are sufficient to excite one or several RE cells to fire.

It is important to mention that a spindle wave also could be started by excitatory stimulation of RE cells whereas the same stimuli on TC cells were much less effective (not shown). This suggests that spindles elicited by cortical stimulation are recruited through excitation of RE cells and their subsequent inhibitory effect on TC cells, consistent with the powerful effect of the cortex in synchronizing spindles in vivo (Contreras and Steriade 1996).

HOW DO SPINDLES PROPAGATE? A recent investigation of spindle waves in ferret thalamic slices (Kim et al. 1995) demonstrated that these oscillations propagate through the divergence of axonal connections between TC and RE cells. At each cycle of the oscillation in the model, the spindle propagated as more TC and RE cells were recruited. A steady propagation occurred only if the projections between TC and RE cells were organized topographically, as appears to be the case from morphological studies (Gonzalo-Ruiz and Lieberman 1995; Minderhoud 1971; Sanderson 1971).

Spindle waves examined on a finer spatial scale consisted of distinct clusters of activity that propagated across the network (Fig. 12); these were similar to the patterns described in a closely related model (Golomb et al. 1996).

These patterns are a consequence of the subharmonic bursting properties of TC cells. The network segregated into groups of TC cells discharging in alternation, as seen in the simple four-cell model (Fig. 7). In the 100-cell model, the spindle started at one or more cells in a localized focus, which evoked the discharge of a localized group of RE and TC cells. This group in turn initiated the discharge of additonal groups of TC and RE cells, leading to propagation of burst activity. A group that just discharged stayed quiescent during the next cycle, at the same time that neighboring groups were discharging. This resulted in clusters of neurons firing in alternation as in Fig. 12.

HOW DO SPINDLES TERMINATE? There are several possible explanations. First, the observed refractoriness (Kim et al. 1995) of the thalamic network implies that there is a process that builds up and subsequently suppresses these oscillations. As proposed previously, an activity-dependent upregulation of $I_h$ might fill this role (Bal and McCormick 1996; Destexhe et al. 1993b; McCormick 1992; Toth and Crunelli 1992). Second, the termination might result from the progressive hyperpolarization of RE cells during a spindle sequence (von Krosigk et al. 1993). Third, there might be an activity-dependent depression of GABAergic currents (Kim et al. 1995; von Krosigk and McCormick 1992). Fourth, in vivo data indicate that the waning of spindle waves is associated with a progressive desynchronization of the network (Contreras and Steriade 1996), although this also could be a natural consequence of waning properties intrinsic to TC cells.

In this paper, we explored the first of these possibilities. The upregulation of $I_h$ is consistent with a series of experimental results: *1*) a few TC cells can display intrinsic waxing-and-waning oscillations (Leresche et al. 1991), and those are sensitive to manipulations of $I_h$ (Soltesz et al. 1991). These oscillations are characterized by an ADP that lasts several seconds (Leresche et al. 1991). *2*) A cesium-sensitive ADP also was observed in TC cells after a spindle sequence, consistent with an augmentation of $I_h$ conductance (Bal and McCormick 1996). *3*) A progressive diminution of input resistance was measured in TC cells during the spindle oscillation in vivo (Nunez et al. 1992). *4*) Spindles triggered by electrical stimulation displayed a refractory period, as observed in vitro (Kim et al. 1995) and in vivo from cortically elicited spindles (D. Contreras, A. Destexhe, T. J. Sejnowski, and M. Steriade, unpublished observations). *5*) Colliding spindle waves do not cross but rather merge into a unique oscillation (Kim et al. 1995). *6*) Spindle oscillations can be transformed into sustained oscillations following extracellular application of cesium (Bal and McCormick 1995), most likely through a block of $I_h$. Taken together, these data are consistent with a progressive build-up of $I_h$ during the spindle oscillation until the TC cells can no longer be sufficiently hyperpolarized to generate rebound bursts. The changes in $I_h$ may be calcium dependent, as we have assumed, or due to another second messenger system (see below).

Another possibility for spindle termination is an enhancement of $I_h$ primarily due to its own activation kinetics. As shown earlier (Destexhe and Babloyantz 1993), voltage-clamp data on $I_h$ reveal a coexistence between fast and slow processes that can be reproduced assuming two independent activation gates. In the presence of other currents, this dual activation kinetics can give rise to waxing-and-waning oscillations followed by an ADP without the need of calcium regulation (Destexhe and Babloyantz 1993; Destexhe et al. 1993a).

Although an upregulation of $I_h$ can account for spindle termination, it does not exclude the other mechanisms mentioned above, as different factors might contribute and reinforce the robustness of the waxing-and-waning process.

### *Paroxysmal oscillations*

Numerous studies have suggested that some types of generalized epileptic seizures may result from a perversion of spindle oscillations (see Avoli et al. 1990 for a review; see also Steriade et al. 1993b). Antagonists of the $GABA_B$ receptor have been found effective in preventing the development of spike-and-wave discharges in some animal models (Hosford et al. 1992; Liu et al. 1992), suggesting that $GABA_B$ receptors are involved critically in the cellular mechanisms of this rhythmicity. This hypothesis was supported further by experiments in ferret thalamic slices, which demonstrated the transformation of spindle oscillations into slower and more synchronized oscillations in the presence of $GABA_A$ antagonists (von Krosigk et al. 1993). These oscillations were abolished by $GABA_B$ antagonists, confirming that they were generated by mechanisms involving $GABA_B$ receptors. These studies are compatible with the idea that intrathalamic $GABA_B$-mediated inhibition plays a role in generalized epileptic patterns.

Several other pharmacological manipulations provide guidance regarding possible mechanisms for paroxysmal oscillations. Both TC and RE neurons generate prolonged burst discharges after application of $GABA_A$ receptor antagonists in vitro (Bal et al. 1995a,b; Huguenard and Prince 1994a,b; Soltesz and Crunelli 1992; von Krosigk et al. 1993). Reinforcing the lateral inhibition in the RE nucleus tended to diminish the occurrence of burst discharges; this mechanism was proposed as a mechanism underlying the action of some antiabsence drugs, such as clonazepam (Huguenard and Prince 1994a).

The present model is fully consistent with these data and emphasizes the critical role of the activation characteristics of $GABA_B$-receptor-mediated currents. Typically, strong stimuli are needed to activate detectable $GABA_B$-mediated currents, as seen in thalamic (Huguenard and Prince 1994b; Sánchez-Vives et al. 1995) and hippocampal slices (Davies et al. 1990; Dutar and Nicoll 1988). This property, as well as the stimulus dependency of $GABA_B$ responses, can be reproduced from the activation kinetics of the G-protein transduction mechanisms underlying the activation of $K^+$ channels associated to $GABA_B$ receptors (Destexhe and Sejnowski 1995). If the independent binding of several G-protein subunits is needed to activate these $K^+$ channels, then the resulting responses have all the properties as determined in hippocampal and thalamic slices. This is consistent with kinetic studies of G-protein action on other systems that showed the involvement of several G-protein binding sites (Boland and Bean 1993; Golard and Siegelbaum 1993; Yamada et al. 1993). A similar conclusion about the need for

cooperative activation of $GABA_B$ responses also was reached independently in another modeling study (Golomb et al. 1996).

At the network level, the model emphasizes the critical role of $GABA_A$ receptors that mediate the lateral inhibition between RE cells (Destexhe and Sejnowski 1995). In the presence of lateral inhibition, RE cells discharge with a rather small number of spikes per burst (Bal et al. 1995b; Huguenard and Prince 1994b). These discharges are insufficient to evoke strong $GABA_B$ currents, and the IPSPs on TC cells are dominated by the $GABA_A$ component (Fig. 2*A2*). In the absence of lateral inhibition, RE cells produce prolonged burst discharges that evoke a prominent $GABA_B$ component in the IPSPs of the target TC cells (Fig. 2*A3*). These results are in agreement with experiments in thalamic slices (Huguenard and Prince 1994a; Sánchez-Vives et al. 1995).

The TC-RE network with suppressed $GABA_A$-mediated inhibition displayed a slower type of waxing-and-waning oscillation at a frequency of 3–4 Hz (Figs. 8 and 9), similar to bicuculline-induced oscillations. These oscillations have similar mechanisms for initiation, propagation, and termination as discussed above for spindle oscillations, but some properties differ. First, all TC cells burst in synchrony; this is due to the strong $GABA_B$ IPSPs that deinactivate $I_T$ more completely and subsequently promote the production of secure rebound bursts. Second, the two cell types produce stronger burst discharges, for the same reasons. Third, the ADP produced in TC cells is of higher amplitude than during spindles, due to the stronger activation of $I_T$ and therefore a more pronounced upregulation of $I_h$. Fourth, the interspindle silent period is longer than during spindles, due to longer recovery after a more pronounced upregulation of $I_h$. Fifth, the propagation velocity is slower, due here to the slower oscillation frequency. All these properties have been observed in thalamic slices (Kim et al. 1995) and occurred in the model because of the activity-dependent upregulation of $I_h$, as discussed above for spindle generation.

The model only replicated qualitatively the difference of propagation velocity between spindle and bicuculline-induced oscillations. Larger differences were observed in the model due to the oversimplified patterns of connectivity and the assumption that all synaptic conductances were the same. However, we expect that fewer synaptic contacts would be made at farther distances, which would result in synaptic weights effectively decaying with distance. Under these conditions, strong $GABA_B$-mediated IPSPs should recruit larger portions of tissue as observed experimentally (Kim et al. 1995). This effect was analyzed in detail in a previous model (Golomb et al. 1996).

The model was able to reproduce accurately the oscillation patterns seen after local application of bicuculline in the RE nucleus (not shown). This application resulted in oscillations intermediate between spindles and bicuculline-induced oscillations; there were more prominent $GABA_B$ IPSPs in TC cells but the frequency was still close to that of spindles (Bal and McCormick, unpublished observations).

The present model suggests a mechanism for the generation of highly synchronized oscillatory discharges at ~3 Hz. After removal of $GABA_A$-mediated inhibition, the disinhibited RE cells generated prolonged burst discharges in response to EPSPs. These prolonged discharges evoked powerful $GABA_B$-mediated IPSPs in TC cells, due to the particular properties of $GABA_B$ transduction mechanisms. After these slow IPSPs, TC cells generated robust rebound bursts that re-excited RE cells and restarted the cycle. The consequence was an oscillation ~3 Hz with higher synchrony than spindle waves.

All of the models reported here have neglected the influence of cortical inputs on thalamic oscillations. Preliminary results (A. Destexhe, unpublished data) indicate that a reduction of cortical inhibition can evoke similar prolonged burst patterns in the thalamus. After diminished $GABA_A$ inhibition in the cortex, thalamically projecting cortical cells can produce very strong discharges, which in turn evoke prolonged bursts in RE cells despite the presence of intact intra-RE inhibition. As described above, prolonged bursts in the RE nucleus can evoke very powerful $GABA_B$-dominated IPSPs in TC cells. The rebound burst in TC cells then occurs after a period of ~300 ms. If the TC rebound can re-excite strong cortical discharges, then this mechanism would lead to ~3-Hz oscillations in the entire thalamocortical circuit. These preliminary results may explain the observation that diffuse application of penicillin, a $GABA_A$ receptor antagonist, to the cerebral cortex can result in spike and wave discharges (Gloor et al. 1990). Models are presently under investigation to test this explanation for generalized epileptic patterns.

### *Predictions of the model*

A series of predictions are generated by the model that could be verified by experiments.

First, the resting membrane potential for TC cells, around −60 mV in the model, should be more depolarized that of RE cells, which should be −70 mV or lower. Under these conditions, TC and RE cells interconnected with glutamatergic and GABAergic synapses would set up a highly excitable structure for generating sustained oscillations, a conclusion also reached in other modeling studies (Destexhe et al. 1993b; Golomb et al. 1996). These predictions are consistent with intracellular recordings in both types of cells during spindle oscillations (Bal et al. 1995a,b; Huguenard and Prince 1992, 1994b). However, the difference seen in experiments is not as large as needed in the model, presumably because RE cells were modeled as single compartments. There is evidence for dendritic $I_T$ in RE cells (Destexhe et al. 1996; Mulle et al. 1986), which may allow burst discharges to be evoked by EPSPs even if the soma is more depolarized.

Second, we predict that an intrinsic mechanism exists in TC cells to control the waning of spindle oscillations (see also Destexhe et al. 1993b). In particular, we suggest that there may be an activity-dependent enhancement of $I_h$. The visible consequences of such an augmentation of $I_h$ is an ADP in TC cells after a spindle sequence, and a higher-amplitude ADP after a sequence of bicuculline-induced oscillations. There must be a slow recovery to account for the observed period of refractoriness (Kim et al. 1995). If $I_h$ accounts for the waning of the oscillation, reduction of this current should lead to sustained oscillations (Fig. 14*C*). Preliminary data have indeed verified this prediction (Bal and McCormick 1996).

Third, we predict that the biophysical mechanism underlying the enhancement of $I_h$ is mediated via intracellular calcium. This is based on evidence for a $Ca^{2+}$ modulation of $I_h$ in sino-atrial node cells (Hagiwara and Irisawa 1989) and neocortical pyramidal neurons (Schwindt et al. 1992). The possible regulation of $I_h$ channels by $Ca^{2+}$ has not yet been investigated in thalamic neurons. $Ca^{2+}$ ions may not bind directly to $I_h$ channels (Zaz et al. 1991) and an indirect modulation is more likely. Cyclic AMP may be a good candidate because $Ca^{2+}$ is involved actively in regulating adenylate cyclase activity (reviewed in MacNeil et al. 1985), and $I_h$ is sensitive to cyclic AMP (Akasu and Tokimasa 1992; DiFrancesco and Mangoni 1994; McCormick and Pape 1990b). The kinetics of this indirect modulation must be slow, similarly to the $Ca^{2+}$-dependent regulation of other types of channels. For example, a kinetic analysis of the slow inactivation of NMDA receptors by intracellular $Ca^{2+}$ (Legendre et al. 1993) reported relatively fast binding and very slow unbinding rates (time constant of ~5 s), consistent with the values we have used here for $I_h$. Our model predicts that the intracellular side of the $I_h$ channel protein should reveal binding sites for calcium-binding proteins or cyclic AMP.

Fourth, a major prediction of our model is that a few cells must be intrinsic oscillators in the network. If a subset of TC cells, of RE cells, or both, are spontaneous oscillators, then the model predicts initiation, propagation, and termination of spindle waves compatible with experimental results. In this study we explored the possibility that a few—as few as one—TC cells produce intrinsic waxing-and-waning oscillations. A few examples of such TC cells have been recorded from cats in vitro (Leresche et al. 1991). The existence of such spontaneous waxing-and-waning TC cells has not yet been investigated in ferret thalamic slices, but spontaneous spindle oscillations typically started at the same foci (Kim et al. 1995), consistent with our hypothesis. We predict that recording in one of these foci after the block of synaptic connections should reveal spontaneously oscillating TC cells.

Fifth, the model suggests that axonal projections in the thalamus should spread into restricted areas instead of running through the whole thalamus. In addition, there should be a topographical organization of axonal projections between TC and RE nuclei such that a local region sends axons to the same region from which it receives afferents. This is consistent with morphological studies showing that in the thalamus, axonal projections arising from TC or RE cells extend at most >100–500 $\mu$m (Cucchiaro et al. 1991; Harris 1981; Jones 1985; Pinault et al. 1995; Uhlrich et al. 1991), and with a topographic organization between reticular thalamus and other nuclei (Fitzgibbon et al. 1995; Gonzalo-Ruiz and Lieberman 1995; Liu et al. 1995; Minderhoud 1971; Ohara and Lieberman 1985; Sanderson 1971).

Sixth, if the connections between the thalamus and associated areas of the cortex also are organized topographically, then signs of propagating oscillation, as well as refractory period, should be observable in multielectrode cortical recordings. Propagation of spindle activity was described in the cortex and thalamus in vivo (Andersen and Andersson, 1968; Verzeano and Negishi 1960; Verzeano et al. 1965) and experiments on anesthetized cats in vivo indicate signs of propagation and refractory period for spindles elicited by cortical stimulation (D. Contreras, A. Destexhe, T. J. Sejnowski, and M. Steriade, unpublished observations). However, many spontaneous spindle sequences appear to have occured nearly simultaneously in cortical sites separated by ≤7 mm (Contreras et al. 1995).

Finally, the model predicts the spatiotemporal organization of spontaneous oscillations. Spindle waves consisted in a series of localized clusters of activity, which propagated through the network with the same velocity as the wavefront (Fig. 12). This property was due to the localized axonal projections combined with the subharmonic bursting properties of TC cells. On the other hand, bicuculline-induced oscillations did not display this phenomenon, but showed more homogeneous patterns of discharge (Fig. 13). If a time resolution of ~10 ms can be achieved, it should be possible to observe this phenomenon using optical recordings in ferret thalamic slices with voltage-sensitive dyes.

We acknowledge U. Kim for discussion.

This research was supported by the Medical Research Council of Canada, Fonds de la Recherche en Santé du Québec, the Klingenstein Fund, the National Institutes of Health, and the Howard Hughes Medical Institute.

Address for reprint requests: A. Destexhe, Dept. of Physiology, Laval University School of Medicine, Quebec G1K 7P4, Canada.

Received 3 January 1996; accepted in final form 28 March 1996.

## REFERENCES

ANDERSEN, P. AND ANDERSSON, S. A. *The Physiological Basis of the Alpha Rhythm.* New York: Appelton Century Crofts, 1968.

ANDERSEN, P. AND RUTJORD, T. Simulation of a neuronal network operating rhythmically through recurrent inhibition. *Nature Lond.* 204: 289–290, 1964.

AKASU, T. AND TOKIMASA, T. Cellular metabolism regulating H and M currents in bullfrog sympathetic ganglia. *Can. J. Physiol. Pharmacol.* 70 *Suppl.*: S51–S55, 1992.

AVOLI, M., GLOOR, P., KOSTOPOULOS, G., AND NAQUET, R. (Editors). *Generalized Epilepsy.* Boston, MA: Birkhauser, 1990.

BAL, T. AND MCCORMICK, D. A. Mechanisms of oscillatory activity in guinea-pig nucleus reticularis thalami in vitro: a mammalian pacemaker. *J. Physiol. Lond.* 468: 669–691, 1993.

BAL, T. AND MCCORMICK, D. A. What stops synchronized thalamocortical oscillations? *Neuron.* In press.

BAL, T., VON KROSIGK, M., AND MCCORMICK, D. A. Synaptic and membrane mechanisms underlying synchronized oscillations in the ferret LGNd in vitro. *J. Physiol. Lond.* 483: 641–663, 1995a.

BAL, T., VON KROSIGK, M., AND MCCORMICK, D. A. Role of the ferret perigeniculate nucleus in the generation of synchronized oscillations in vitro. *J. Physiol. Lond.* 483: 665–685, 1995b.

BOLAND, L. M. AND BEAN, B. P. Modulation of N-type calcium channels in bullfrog sympathetic neurons by luteinizing hormone-releasing hormone: kinetics and voltage dependence. *J. Neurosci.* 13: 516–533, 1993.

CLEMENTS, J. D., LESTER, R. A. J., TONG, J., JAHR, C., AND WESTBROOK, G. L. The time course of glutamate in the synaptic cleft. *Science Wash. DC* 258: 1498–1501, 1992.

COLQUHOUN, D., JONAS, P., AND SAKMANN, B. Action of brief pulses of glutamate on AMPA/KAINATE receptors in patches from different neurons of rat hippocampal slices. *J. Physiol. Lond.* 458: 261–287, 1992.

CONTRERAS, D., DESTEXHE, A., SEJNOWSKI, T. J., AND STERIADE, M. Synchronization of thalamic spindle oscillations is enhanced by cortical feedback input. *Soc. Neurosci. Abstr.* 21: 1187, 1995.

CONTRERAS, D. AND STERIADE, M. Spindle oscillation in cats: the role of corticothalamic feedback in a thalamically-generated rhythm. *J. Physiol. Lond.* 490: 159–179, 1996.

COULTER, D. A., HUGUENARD, J. R., AND PRINCE, D. A. Calcium currents in rat thalamocortical relay neurones: kinetic properties of the transient, low-threshold current. *J. Physiol. Lond.* 414: 587–604, 1989.

CUCCHIARO, J. B., UHLRICH, D. J., AND SHERMAN, S. M. Electron-micro-

scopic analysis of synaptic input from the perigeniculate nucleus to the A-laminae of the lateral geniculate nucleus in cats. *J. Comp. Neurol.* 310: 316–336, 1991.

DAVIES, C. H., DAVIES, S. N., AND COLLINGRIDGE, G. L. Paired-pulse depression of monosynaptic GABA-mediated inhibitory postsynaptic responses in rat hippocampus. *J. Physiol. Lond.* 424: 513–531, 1990.

DESTEXHE, A. AND BABLOYANTZ, A. A model of the inward current $I_h$ and its possible role in thalamocortical oscillations. *NeuroReport* 4: 223–226, 1993.

DESTEXHE, A., BABLOYANTZ, A., AND SEJNOWSKI, T.J. Ionic mechanisms for intrinsic slow oscillations in thalamic relay neurons. *Biophys. J.* 65: 1538–1552, 1993a.

DESTEXHE, A., BAL, T., MCCORMICK, D. A., AND SEJNOWSKI, T. J. Ionic mechanisms underlying synchronized oscillations and traveling waves in a model of ferret thalamic slices. *Soc. Neurosci. Abstr.* 21: 1187, 1995.

DESTEXHE, A., CONTRERAS, D., SEJNOWSKI, T. J., AND STERIADE, M. A model of spindle rhythmicity in the isolated thalamic reticular nucleus. *J. Neurophysiol.* 72: 803–818, 1994a.

DESTEXHE, A., CONTRERAS, D., SEJNOWSKI, T. J., AND STERIADE, M. Modeling the control of reticular thalamic oscillations by neuromodulators. *NeuroReport* 5: 2217–2220, 1994b.

DESTEXHE, A., CONTRERAS, D., STERIADE, M., SEJNOWSKI, T. J., AND HUGUENARD, J. R. In vivo, in vitro and computational analysis of dendritic calcium currents in thalamic reticular neurons. *J. Neurosci.* 16: 169–185, 1996.

DESTEXHE, A., MAINEN, Z., AND SEJNOWSKI, T. J. An efficient method for computing synaptic conductances based on a kinetic model of receptor binding. *Neural Comput.* 6: 14–18, 1994c.

DESTEXHE, A., MAINEN, Z., AND SEJNOWSKI, T. J. Synthesis of models for excitable membranes, synaptic transmission and neuromodulation using a common kinetic formalism. *J. Comput. Neurosci.* 1: 195–230, 1994d.

DESTEXHE, A., MCCORMICK, D. A., AND SEJNOWSKI, T. J. A model for 8–10 Hz spindling in interconnected thalamic relay and reticularis neurons. *Biophys. J.* 65: 2474–2478, 1993b.

DESTEXHE, A. AND SEJNOWSKI, T. J. G-protein activation kinetics and spillover of GABA may account for differences between inhibitory responses in the hippocampus and thalamus. *Proc. Natl. Acad. Sci. USA* 92: 9515–9519, 1995.

DESTEXHE, A. AND SEJNOWSKI, T. J. Synchronized oscillations in thalamic networks: insights from modeling studies. In: *Thalamus,* edited by M. Steriade, E. G. Jones, and D. A. McCormick. Amsterdam: Elsevier. In press.

DIFRANCESCO, D. AND MANGONI, M. Modulation of single hyperpolarization-activated channels (i(f)) by cAMP in the rabbit sino-atrial node. *J. Physiol. Lond.* 474: 473–482, 1994.

DUTAR, P. AND NICOLL, R. A. A physiological role for GABAB receptors in the central nervous system. *Nature Lond.* 332: 156–158, 1988.

FITZGIBBON, T., TEVAH, L. V., AND JERVIE-SEFTON, A. Connections between the reticular nucleus of the thalamus and pulvinar-lateralis posterior complex: a WGA-HRP study. *J. Comp. Neurol.* 363: 489–504, 1995.

GLOOR, P., AVOLI, M., AND KOSTOPOULOS, G. Thalamocortical relationships in generalized epilepsy with bilateral synchronous spike-and-wave discharge. In: *Generalized Epilepsy,* edited by M. Avoli, P. Gloor, G. Kostopoulos, and R. Naquet. Boston, MA: Birkhauser, 1990, p. 190–212.

GOLARD, A. AND SIEGELBAUM, S. A. Kinetic basis for the voltage-dependent inhibition of N-type calcium current by somatostatin and norepinephrine in chick sympathetic neurons. *J. Neurosci.* 13: 3884–3894, 1993.

GOLOMB, D., WANG, X. J., AND RINZEL, J. Synchronization properties of spindle oscillations in a thalamic reticular nucleus model. *J. Neurophysiol.* 72: 1109–1126, 1994.

GOLOMB, D., WANG, X. J., AND RINZEL, J. Propagation of spindle waves in a thalamic slice model. *J. Neurophysiol.* 75: 750–769, 1996.

GONZALO-RUIZ, A. AND LIEBERMAN, A. R. Topographic organization of projections from the thalamic reticular nucleus to the anterior thalamic nuclei in the rat. *Brain Res. Bull.* 37: 17–35, 1995.

HAGIWARA, N. AND IRISAWA, H. Modulation by intracellular $Ca^{2+}$ of the hyperpolarization-activated inward current in rabbit single sino-atrial node cells. *J. Physiol. Lond.* 409: 121–141, 1989.

HARRIS, R. M. Axon collaterals in the thalamic reticular nucleus from thalamocortical neurons of the rat ventrobasal thalamus. *J. Comp. Neurol.* 258: 397–406, 1987.

HINES, M. NEURON—A program for simulation of nerve equations. In: *Neural Systems: Analysis and Modeling,* edited by F. Eeckman. Boston: Kluwer Academic Publishers, 1993, p. 127–136.

HODGKIN, A. L. AND HUXLEY, A. F. A quantitative description of membrane current and its application to conduction and excitation in nerve. *J. Physiol. Lond.* 117: 500–544, 1952.

HOSFORD, D. A., CLARK, S., CAO, Z., WILSON, W. A., JR., LIN, F. H., MORRISETT, R. A., AND HUIN, A. The role of $GABA_B$ receptor activation in absence seizures of lethargic (lh/lh) mice. *Science Wash. DC* 257: 398–401, 1992.

HUGUENARD, J. R., COULTER, D. A., AND PRINCE, D. A. A fast transient potassium current in thalamic relay neurons: kinetics of activation and inactivation. *J. Neurophysiol.* 66: 1305–1315, 1991.

HUGUENARD, J. R., AND MCCORMICK, D. A. Simulation of the currents involved in rhythmic oscillations in thalamic relay neurons. *J. Neurophysiol.* 68: 1373–1383, 1992.

HUGUENARD, J. R. AND PRINCE, D. A. A novel T-type current underlies prolonged $Ca^{2+}$-dependent bursts firing in GABAergic neurons of rat thalamic reticular nucleus. *J. Neurosci.* 12: 3804–3817, 1992.

HUGUENARD, J. R. AND PRINCE, D. A. Clonazepam suppresses $GABA_B$-mediated inhibition in thalamic relay neurons through effects in nucleus reticularis. *J. Neurophysiol.* 71: 2576–2581, 1994a.

HUGUENARD, J. R. AND PRINCE, D. A. Intrathalamic rhythmicity studied in vitro: nominal T-current modulation causes robust anti-oscillatory effects. *J. Neurosci.* 14: 5485–5502, 1994b.

JONES, E. G. *The Thalamus.* New York: Plenum, 1985.

KIM, U., BAL, T., AND MCCORMICK, D. A. Spindle waves are propagating synchronized oscillations in the ferret LGNd in vitro. *J. Neurophysiol.* 74: 1301–1323, 1995.

KOPELL, N. AND LEMASSON, G. Rhythmogenesis, amplitude modulation, and multiplexing in a cortical architecture. *Proc. Natl. Acad. Sci. USA* 91: 10586–10590, 1994.

LEGENDRE, P., ROSENMUND, C., AND WESTBROOK, G. L. Inactivation of NMDA channels in cultured hippocampal neurons by intracellular calcium. *J. Neurosci.* 13: 674–684, 1993.

LERESCHE, N., LIGHTOWLER, S., SOLTESZ, I., JASSIK-GERSCHENFELD, D., AND CRUNELLI, V. Low frequency oscillatory activities intrinsic to rat and cat thalamocortical cells. *J. Physiol. Lond.* 441: 155–174, 1991.

LIU, Z., VERGNES, M., DEPAULIS, A., AND MARESCAUX, C. Involvement of intrathalamic $GABA_B$ neurotransmission in the control of absence seizures in the rat. *Neuroscience* 48: 87–93, 1992.

LIU, X. B., WARREN, R. A., AND JONES, E. G. Synaptic distribution of afferents from reticular nucleus in ventroposterior nucleus of cat thalamus. *J. Comp. Neurol.* 352: 187–202, 1995.

MACNEIL, S., LAKEY, T., AND TOMLINSON, S. Calmodulin regulation of adenylate cyclase activity. *Cell Calcium* 6: 213–216, 1985.

MCCORMICK, D. A. Neurotransmitter actions in the thalamus and cerebral cortex and their role in neuromodulation of thalamocortical activity. *Prog. Neurobiol.* 39: 337–388, 1992.

MCCORMICK, D. A. AND HUGUENARD, J. R. A model of the electrophysiological properties of thalamocortical relay neurons. *J. Neurophysiol.* 68: 1384–1400, 1992.

MCCORMICK, D. A. AND PAPE, H.C. Properties of a hyperpolarization-activated cation current and its role in rhythmic oscillations in thalamic relay neurones. *J. Physiol. Lond.* 431: 291–318, 1990a.

MCCORMICK, D. A. AND PAPE, H. C. Noradrenergic modulation of a hyperpolarization-activated cation current in thalamic relay neurones. *J. Physiol. Lond.* 431: 319–342, 1990b.

MINDERHOUD, J. M. An anatomical study of the efferent connections of the thalamic reticular nucleus. *Exp. Brain Res.* 112: 435–446, 1971.

MORISON, R. S. AND BASSETT, D. L. Electrical activity of the thalamus and basal ganglia in decorticate cats. *J. Neurophysiol.* 8: 309–314, 1945.

MUHLETHALER, M. AND SERAFIN, M. Thalamic spindles in an isolated and perfused preparation in vitro. *Brain Res.* 524: 17–21, 1990.

MULLE, C., MADARIAGA, A., AND DESCHÊNES, M. Morphology and electrophysiological properties of reticularis thalami neurons in cat: in vivo study of a thalamic pacemaker. *J. Neurosci.* 6: 2134–2145, 1986.

NUNEZ, A., CURRO-DOSSI, R., CONTRERAS, D., AND STERIADE, M. Intracellular evidence for incompatibility between spindle and delta oscillations in thalamocortical neurons of cat. *Neuroscience* 48: 75–85, 1992.

OHARA, P.T. AND LIEBERMAN, A. R. The thalamic reticular nucleus of the adult rat: experimental anatomical studies. *J. Neurocytol.* 14: 365–411, 1985.

OTIS, T. S., DEKONINCK, Y., AND MODY, I. Characterization of synaptically elicited $GABA_B$ responses using patch-clamp recordings in rat hippocampal slices. *J. Physiol. Lond.* 463: 391–407, 1993.

OTIS, T. S. AND MODY, I. Modulation of decay kinetics and frequency of

$GABA_A$ receptor-mediated spontaneous inhibitory postsynaptic currents in hippocampal neurons. *Neuroscience* 49: 13–32, 1992.

PINAULT, D., BOURASSA, J., AND DESCHÊNES, M. The axonal arborization of single thalamic reticular neurons in the somatosensory thalamus of the rat. *Eur. J. Neurosci.* 7: 31–40, 1995.

PRESS, W. H., FLANNERY, B. P., TEUKOLSKY, S. A., AND VETTERLING, W. T. *Numerical Recipes. The Art of Scientific Computing.* Cambridge: Cambridge University Press, 1986.

RUSH, M. E. AND RINZEL, J. Analysis of bursting in a thalamic neuron model. *Biol. Cybern.* 71: 281–291, 1994.

SÁNCHEZ-VIVES, M.V., BAL, T., AND MCCORMICK, D. A. Properties of GABAergic inhibition in the ferret LGNd contributing to the generation of synchronized oscillations. *Soc. Neurosci. Abstr.* 21: 11, 1995.

SANDERSON, K.J. The projection of the visual field to the lateral geniculate and medial interlaminar nuclei in the cat. *J. Comp. Neurol.* 143: 101–108, 1971.

SCHWINDT, P. C., SPAIN, W. J., AND CRILL, W. E. Effects of intracellular calcium chelation on voltage-dependent and calcium-dependent currents in cat neocortical neurons. *Neuroscience* 47: 571–578, 1992.

SOLTESZ, I. AND CRUNELLI, V. GABAA and pre- and post-synaptic GABAB receptor-mediated responses in the lateral geniculate nucleus. *Prog. Brain Res.* 90: 151–169, 1992.

SOLTESZ, I., LIGHTOWLER, S., LERESCHE, N., JASSIK-GERSCHENFELD, D., POLLARD, C. E., AND CRUNELLI, V. Two inward currents and the transformation of low frequency oscillations of rat and cat thalamocortical cells. *J. Physiol. Lond.* 441: 175–197, 1991. STERIADE, M., CURRO DOSSI, R., AND CONTRERAS, D. Electrophysiological properties of intralaminar thalamocortical cells discharging rhythmic (approximately 40 HZ) spike-bursts at approximately 1000 HZ during waking and rapid eye movement sleep. *Neuroscience* 56: 1–9, 1993a.

STERIADE, M. AND DESCHÊNES, M. The thalamus as a neuronal oscillator. *Brain Res. Rev.* 8: 1–63, 1984.

STERIADE, M., DESCHÊNES, M., DOMICH, L., AND MULLE, C. Abolition of spindle oscillations in thalamic neurons disconnected from nucleus reticularis thalami. *J. Neurophysiol.* 54: 1473–1497, 1985.

STERIADE, M., DOMICH, L., OAKSON, G., AND DESCHÊNES, M. The deafferented reticular thalamic nucleus generates spindle rhythmicity. *J. Neurophysiol.* 57: 260–273, 1987.

STERIADE, M., JONES, E. G, AND MCCORMICK, D. A. (Editors). *Thalamus.* Amsterdam: Elsevier. In press.

STERIADE, M. AND LLINÁS, R. R. The functional states of the thalamus and the associated neuronal interplay. *Physiol. Rev.* 68: 649–742, 1988.

STERIADE, M., MCCORMICK, D. A., AND SEJNOWSKI., T. J. Thalamocortical oscillations in the sleeping and aroused brain. *Science Wash. DC* 262: 679–685, 1993b.

TOTH, T. AND CRUNELLI, V. Modelling spindle-like oscillations in thalamocortical neurones. *Soc. Neurosci. Abstr.* 18: 1018, 1992.

TRAUB, R. D. AND MILES, R. *Neuronal Networks of the Hippocampus.* Cambridge: Cambridge University Press, 1991.

UHLRICH, D. J., CUCCHIARO, J. B., HUMPHREY, A. L., AND SHERMAN, S. M. Morphology and axonal projection patterns of individual neurons in the cat perigeniculate nucleus. *J. Neurophysiol.* 65: 1528–1541, 1991.

VERZEANO, M., LAUFER, M., SPEAR, P., AND MCDONALD, S. L'activite des reseaux neuroniques dans le thalamus du singe. *Actual. Neurophysiol.* 6: 223–251, 1965.

VERZEANO, M. AND NEGISHI, K. Neuronal activity in cortical and thalamic networks. A study with multiple microelectrodes. *J. Gen. Physiol.* 43: 177–195, 1960.

VON KROSIGK, M., BAL, T., AND MCCORMICK, D. A. Cellular mechanisms of a synchronized oscillation in the thalamus. *Science Wash. DC* 261: 361–364, 1993.

VON KROSIGK, M. AND MCCORMICK, D. A. Mechanisms of frequency dependent facilitation of corticothalamic EPSPs. *Soc. Neurosci. Abstr.* 18: 140, 1992.

WANG, X. J. Multiple dynamical modes of thalamic relay neurons: rhythmic bursting and intermittent phase-locking. *Neuroscience* 59: 21–31, 1994.

WARREN, R. A., AGMON, A., AND JONES, E. G. Oscillatory synaptic interactions between ventroposterior and reticular neurons in mouse thalamus in vitro. *J. Neurophysiol.* 72: 1993–2003, 1994.

XIANG, Z., GREENWOOD, A. C., AND BROWN, T. Measurement and analysis of hippocampal mossy-fiber synapses. *Soc. Neurosci. Abstr.* 18: 1350, 1992.

YAMADA, M., JAHANGIR, A., HOSOYA, Y., INANOBE, A., KATADA, T., AND KURACHI, Y. GK* and brain G beta gamma activate muscarinic $K^+$channel through the same mechanism. *J. Biol. Chem.* 268: 24551–24554, 1993.

ZAZA, A., MACCAFERRI, G., MANGONI, M., AND DIFRANCESCO, D. Intracellular calcium does not directly modulate cardiac pacemaker (if) channels. *Pflueg. Archiv. Eur. J. Physiol.* 419: 662–664, 1991.